A Minimalist Dynamic Climbing Robot: Modeling, Analysis and Experiments

Amir Degani

June 19, 2009

Thesis Proposal
CMU-RI-TR-09-28

Thesis Committee:
Matthew T. Mason, Co-Chair
Howie Choset, Co-Chair
Christopher G. Atkeson
Kevin M. Lynch, Northwestern University
Andy Ruina, Cornell University

The Robotics Institute
Carnegie Mellon University
Pittsburgh, PA 15213

Copyright © 2009 Amir Degani

Keywords: Climbing Robot, Dynamic Locomotion, Minimalist Robot, Open-loop, Nonlinear Analysis

Abstract

Dynamics in locomotion is highly useful, as can be seen in animals and gradually in robots. For instance, chimpanzees are dynamic climbers that can reach virtually any part of a tree and even move to neighboring trees, while sloths are quasistatic climbers confined only to a few branches. Although dynamic maneuvers are undoubtedly beneficial, only a few engineered systems use them. This is because the design and control are often extremely complicated. Moreover, these dynamic robots mostly locomote horizontally.

This work extends dynamic robotic legged locomotion from horizontal motions such as walking, hopping, and running, to vertical motions such as leaping maneuvers. The proposed mechanism, called DSAC for Dynamic, Single Actuated Climber, resembles the motion of an athlete jumping and climbing inside a chute. Whereas this environment is an unnavigable obstacle for a slow, quasistatic climber, it is an invaluable source of reaction forces for a dynamic climber. The mechanism proposed here will try to achieve dynamic, vertical motion while retaining simplicity in design and control.

DSAC comprises only two links connected by a single oscillating actuator. This simple, open loop motion, almost miraculously propels the robot stably between two vertical walls. A change in the mechanism's parameters not only changes the stability of the system but also changes the climbing pattern.

I propose to use DSAC to explore minimalist approach to locomotion. I propose first to identify the optimal parameters and control for climbing in this open-loop paradigm by studying variations in robot parameters, environment parameters and control input. Only then will I incrementally add feedback and mechanical complexity to achieve climbing in more difficult environments such as piecewise linear walls.

Contents

1 Introduction **1**
- 1.1 Motivation: Why use dynamics? . . . 2
- 1.2 System Description . . . 3
- 1.3 Problem statement and scope of the thesis . . . 6
- 1.4 Document Outline . . . 7

2 Related Work **8**
- 2.1 Minimalism . . . 8
- 2.2 Walking robots . . . 9
- 2.3 Hopping robots . . . 9
- 2.4 Climbing mechanisms . . . 10
  - 2.4.1 Quasistatic climbers . . . 10
  - 2.4.2 Dynamic climbers . . . 10
- 2.5 Open-loop control . . . 11
- 2.6 Planning for dynamic systems . . . 12

3 Background and Preliminaries **13**
- 3.1 General Equations of Motion . . . 13
  - 3.1.1 Lagrangian formulation of equations of motion . . . 13
  - 3.1.2 Lagrange's equations with contact forces . . . 15
  - 3.1.3 State space representation . . . 16
  - 3.1.4 Autonomous system vs. Non-Autonomous Systems . . . 16
  - 3.1.5 Nondimensionalizing Differential Equations . . . 17
- 3.2 Nonlinear analysis . . . 17
  - 3.2.1 Orbital stability - the Poincaré map . . . 18
  - 3.2.2 Stability definition . . . 20
  - 3.2.3 Bifurcations of nonlinear systems . . . 23
  - 3.2.4 Types of dynamic motions . . . 23
  - 3.2.5 Methods of analyzing nonlinear systems . . . 24
    - 3.2.5.1 The Poincaré map . . . 24
    - 3.2.5.2 Lyapunov exponents . . . 25
    - 3.2.5.3 Spectrum analysis - Fourier analysis . . . 26

4 Preliminary Results **27**
4.1 Modeling . . . 27
4.1.1 System description and modeling assumptions . . . 27
4.1.2 General equations of motion . . . 30
4.1.2.1 Free flight phase . . . 31
4.1.2.2 Impact phase . . . 32
4.1.2.3 Stance phase . . . 34
4.1.2.4 Summary of modeling . . . 35
4.2 Analysis . . . 35
4.2.1 A typical climbing motion . . . 35
4.2.2 Open loop stability . . . 36
4.2.3 Poincaré map and corresponding Poincaré section . . . 38
4.2.4 Local stability . . . 39
4.2.4.1 Fixed point search . . . 40
4.2.4.2 Linearized Poincaré map and eigenvalues . . . 40
4.3 Analysis results . . . 41
4.3.1 Local stability - varying frequency and amplitude . . . 41
4.3.1.1 Bifurcations . . . 42
4.3.1.2 Power spectrum analysis . . . 44
4.3.1.3 Lyapunov exponents . . . 44
4.3.1.4 Climbing rates . . . 47
4.3.2 Local stability - varying mechanism parameters . . . 47
4.3.2.1 Changing l_s - link ratio . . . 48
4.3.2.2 Summary of analysis results . . . 49
4.4 Initial experiments . . . 51
4.4.1 Experimental setup . . . 51
4.4.2 Current mechanism design . . . 52
4.4.3 Initial proof-of-concept experiments . . . 52
4.5 Summary of initial work . . . 54

5 Proposed Work **59**
5.1 Open-loop stability and implications . . . 59
5.1.1 Improvements and extensions . . . 59
5.1.2 Parameter search . . . 61
5.1.3 Global stability – basin-of-attraction . . . 61
5.1.4 Optimal open-loop control . . . 62
5.2 Uneven terrain – toward piecewise linear walls . . . 62
5.2.1 Control and planning . . . 63
5.2.2 Proposed design . . . 65
5.3 Power efficiency, and more efficient prototypes . . . 65
5.4 Experimental validation . . . 66
5.5 Timeline . . . 67
5.6 Conclusions . . . 68

A Nondimensionalizing **70**
A.1 Nondimensionalizing differential equations 70

B Equations of Motion **72**
B.1 General equations of motion 72
B.1.0.1 Free flight phase 72
B.1.0.2 Impact phase 74
B.1.0.3 Stance phase 75
B.2 Nondimensionalisation of the equations of motion 76

Bibliography **78**

List of Figures

1.1 Human climbing between two vertical walls. . . . 2
1.2 Schematics of the two link mechanism climbing between two parallel walls. . . . 4
1.3 Example of a single contact climbing motion. . . . 4
1.4 Example of a double contact climbing motion. . . . 5

2.1 A few examples of quasistatic climbing mechanisms divided into four groups depending on the "attachment mechanism". . . . 11

3.1 Poincaré map. . . . 20
3.2 The position in the complex plane of the characteristic multipliers 22
3.3 Scenarios depicting how the Floquet multipliers leave the unit circle for different local bifurcations 23

4.1 Schematics of two link mechanism climbing between two parallel walls. . . . 28
4.2 Three phases of climbing gait. . . . 31
4.3 phase plot of a typical climbing motion. . . . 32
4.4 Finding angular momentum around contact point c. . . . 33
4.5 Three phases including flip during impact phase. . . . 35
4.6 phase plot of a typical climbing motion with the flipping action of impact phase. . . 36
4.7 A-ω stability plot. . . . 43
4.8 Bifurcation diagram. . . . 43
4.9 Poincaré plots and power spectrum of $\omega = 15\frac{\text{rad}}{\text{sec}}, 30\frac{\text{rad}}{\text{sec}}$ 45
4.10 Poincaré plots and power spectrum of $\omega = 53.5\frac{\text{rad}}{\text{sec}}, = 56.4\frac{\text{rad}}{\text{sec}}$ 46
4.11 Lyapunov exponents plot. . . . 47
4.12 Averaged climbing rate. . . . 48
4.13 Bifurcation plot - varying l_s. . . . 49
4.14 PSD and Poincaré plots revealing bifurcations with leg length ratio change - l_s . . 50
4.15 Maximum Lyapunov exponent. . . . 51
4.16 Air-table and tracking system mounted above. . . . 52
4.17 Current mechanism design. . . . 54
4.18 Proof-of-concept experiment - $\omega = 15.3\frac{\text{rad}}{\text{sec}}$ – image sequence 1/30 sec apart. . . . 55
4.19 Proof-of-concept experiment - $\omega = 15.3\frac{\text{rad}}{\text{sec}}$ – plot of configuration variables . . . 56
4.20 Proof-of-concept experiment - $\omega = 19\frac{\text{rad}}{\text{sec}}$ – image sequence 1/30 sec apart. . . . 57
4.21 Proof-of-concept experiment - $\omega = 19\frac{\text{rad}}{\text{sec}}$ – plot of configuration variables 58

5.1 Schematics of new two link mechanism climbing between two parallel walls with added parameters. 60
5.2 Constructing the planning graph 64
5.3 Sketch of proposed mechanism design with varying length foot. 66

B.1 Schematics of two link mechanism climbing between two parallel walls (same as Fig. 4.1). 73

Chapter 1

Introduction

The use of dynamics motions in locomotion can help overcome obstacles and increase the feasible foot placement. Dynamic motions are prevalent in nature but not as much in engineered systems. The complexity involved in designing and controlling these systems usually makes them impractical. In this thesis a new mechanism is proposed that achieves these dynamic motions with an extremely simple mechanism. This minimalist mechanism consists of a single open-loop controlled motor connecting two links. The goal of this thesis is to show how dynamic motions can help design a minimalist mechanism and explore this novel, single actuated mechanism which is able to climb vertically between two parallel walls. I believe this mechanism is a good platform to demonstrate how dynamic motions do not inherently imply mechanical complexity, nor do they imply complex control. The proposed future work seeks to find an optimal and efficient climbing mechanism. The future work further explores the possibilities of adding complexity to this system in order to enable climbing in a more complex environment, such as piecewise linear walls.

1.1 Motivation: Why use dynamics?

Humans and even more so animals use dynamic motions in everyday tasks. From running, jumping over obstacles, throwing objects, and climbing. Other than speed, why are dynamic motions superior to slower, quasistatic motions? There are two main reasons. First, being able to overcome obstacles which are impassible while moving slowly. As an example, say a human rock climber tries to hold onto a distant handhold but cannot reach it. One strategy, albeit dangerous, is to leap upwards to try to grab onto the handhold. This is one way to imagine how a dynamic, leaping movement can help increase reachability. Figure 1.1 depicts another example of a human using dynamic motions to climb inside a chute. The second reason that one might use dynamic motions in an articulated, engineered, mechanism is related to minimalism. The use of dynamic movements can reduce the number of active degrees of freedom – a minimalist mechanism. In this manuscript a minimalist mechanism is defined as one that contains a minimum number of active degrees of freedom.

Dynamic locomotion has started to gain popularity in the last few decades in the legged robot field. Initiated by Marc Raibert at CMU, the Leg Lab has built and analyzed many dynamic hopping and running mechanisms. Today, Boston Dynamic's BigDog and Rhex (Saranli et al., 2001) both have impressive abilities to maneuver dynamically over rough terrain. In contrast, climbing machines are far less common.

Although dynamic motions can be superior to the quasistatic ones, it is hard to find such

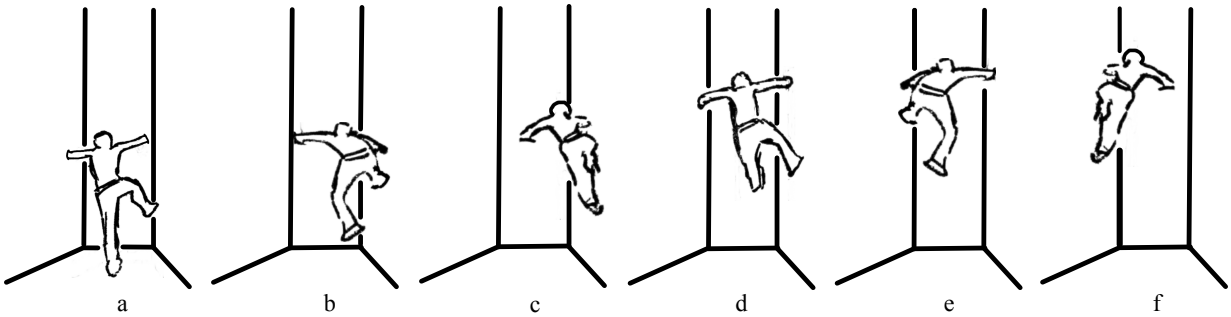

Figure 1.1: Human climbing between two vertical walls.

engineered mechanisms. The reason lies in the complexity of the design. In order to make such a mechanism locomote robustly, it should be designed carefully with high accuracy to reduce uncertainty while moving dynamically and with high powered motors to achieve these dynamic motions. Most importantly these dynamic machines should be controlled at high speeds since the movements are fast. These reasons deter most designers from entering into this realm. Nonetheless, the proposed mechanism can gain from both worlds, its dynamic motion enables fast climbing that can overcome obstacles that its counterpart quasistatic system cannot, while still staying simple in design and robust and stable without any feedback or closed-loop control.

This thesis will describe a minimalist mechanism – DSAC, for Dynamic Single Actuated Climber. The DSAC comprises a single actuated joint connecting two links. By using dynamic motions this mechanism is able to climb up a chute between two parallel walls. I will further propose that by using a simple control algorithm the mechanism can climb in a more complex environment.

1.2 System Description

The proposed mechanism is planar and consists of two links; the first is the main body and the second is the leg. The leg which contacts the wall, is connected to the main body through an actuated revolute joint (Fig. 1.2). I will show that even when the motor outputs a simple symmetric oscillation, such as a sinusoidal, the mechanism, under some parameters' choices, will climb stably. The change in mechanism's parameters alters the behavior of the mechanism significantly. I have identified two "typical" climbing motions: single contact and double contact. The former only contacts the top of the leg, and the latter also contacts the bottom of the leg (see Figs. 1.3 and 1.4, respectively).

The single contact climbing is advantageous in that it can climb wider gaps, however, in general, the frequencies required from the motor are larger than the double contact climbing. On the other hand the double contact climbing is restricted to narrower gaps. Double contact

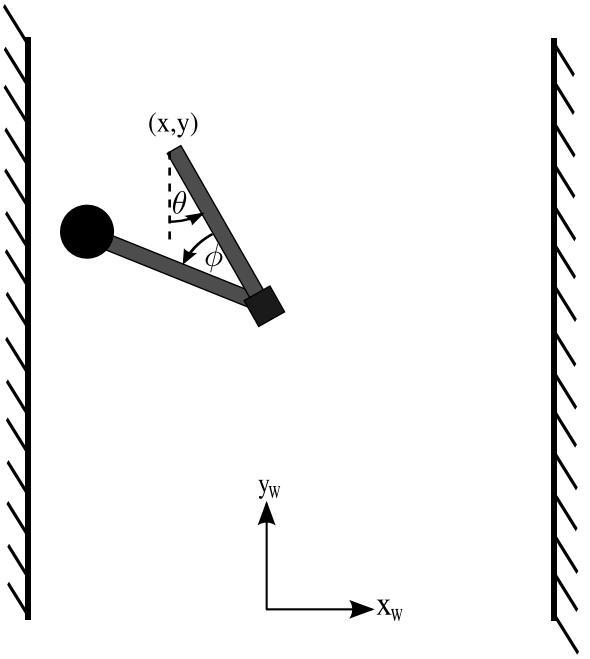

Figure 1.2: Schematics of the two link mechanism climbing between two parallel walls.

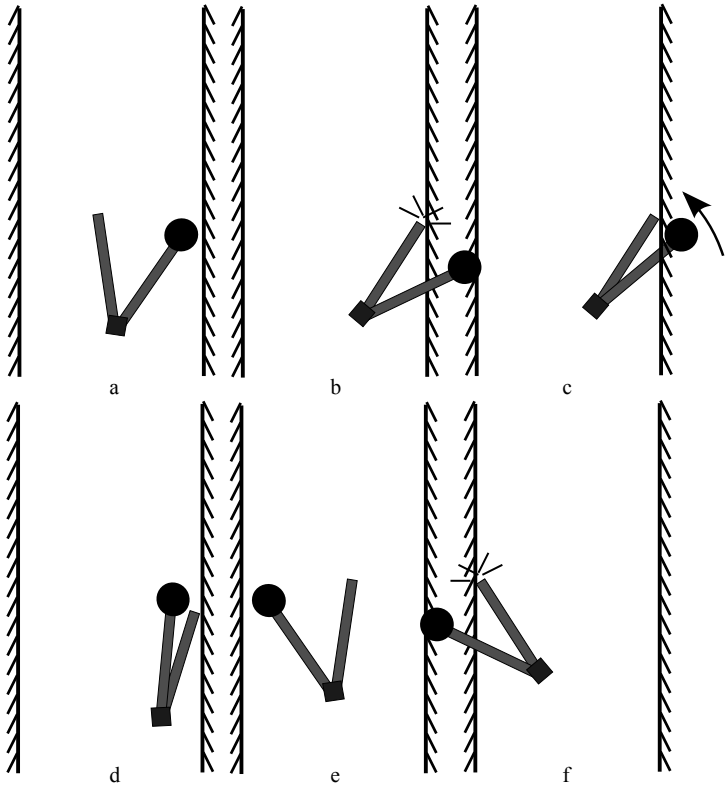

Figure 1.3: Example of a single contact climbing motion.

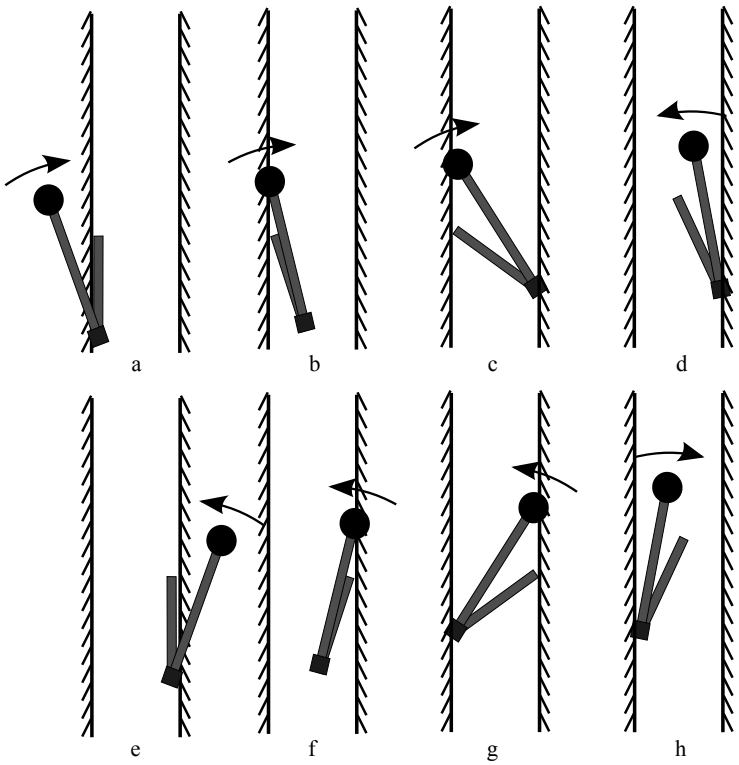

Figure 1.4: Example of a double contact climbing motion.

climbing is less dynamic since most of the climbing motion follows from rotations around the points of contact and not during flight phase. Throughout most of this manuscript I will focus on the more dynamic single contact climbing motion. One might say that the motion of this mechanism is in many senses similar to a human athlete climbing between two walls by pushing off with his legs, as seen in the cartoon in Fig. 1.1.

To help understand how the DSAC climbs, it is helpful to decompose the motion from one wall to the other into three phases; flight, impact and stance (see Fig. 1.3(a,b,c), respectively). The flight phase is just a simple continuous motion without any external forces applied to the body, other than gravity. The impact phase can be regarded as an instantaneous phase where the configuration does not change but the velocities do change instantaneously. The stance phase is the phase where the pendulum-like body swings toward the counter wall and the leg is in contact with the wall.

It is valuable to examine each phase in order to understand how the mechanism is capable of

climbing stably without any sort of control loop. The analysis section will show that during the impact phase, the leg looses most of its angular velocity which acts as a reset function to reduce the accumulated perturbation after each impact. The stance phase has two "tasks". The body swings toward the counter wall which makes the leg "stick" on the wall. While swinging the body, the mechanism absorbs kinetic energy which gives it the kick during the transition to flight phase. The flight phase is the where the mechanism gains height and changes configuration that enable a continuous climbing motion. This motion is further explained more formally in the next chapters. Once again, one might imagine this motion as the human from the cartoon in Fig. 1.1. The kickoff as in Fig. 1.1(c) is equivalent to the stance phase. This phase imparts energy into the system until it transitions to flight phase. Figures 1.1(d,e) resemble the flight and impact phases, respectively.

1.3 Problem statement and scope of the thesis

Statement of intent: *The purpose of this thesis is to explore minimalism in locomotion. More specifically, how the use of dynamic motions can help design a minimalist, climbing mechanism. At this stage in the research, a proof-of-concept of a single actuated mechanism climbing between two parallel walls has been designed, built, and analyzed. I intend to use the current analysis to further explore the possibilities of adding complexity to this system in order to enable climbing in a more complex environment, such as piecewise linear walls.*

I have so far modeled and analyzed the DSAC, a two link, single actuator system and identified interesting changes in dynamics when some of the parameters are changed. This thesis will mostly be exploratory. The proposed work will explore the different DSAC types, such as different masses, lengths, inertias, frequency input etc., in order to find better open-loop climbing characteristics and more stable motions. The work will explore what are the initial conditions leading to a stable climbing motion. Furthermore, the knowledge from the open loop analysis will be used to address more complex environments with just a small addition of feedback and

sensory information. The final goal is to climb between piecewise linear walls using a closed-loop control. The experimental section will correlate the analysis results on an experimental testbed.

1.4 Document Outline

The outline of this document is as follows. Chapter 2 describes related work, including climbing mechanisms, walking machines, hopping robots, planning for dynamic systems, and analysis of dynamic systems. Chapter 3 summarizes the relevant mathematical preliminaries used in succeeding chapters. Chapter 4 summarizes the work done so far. It introduces the model of the mechanism and the analysis. It also shows the experimental setup with initial proof-of-concept experiments. Chapter 5 proposes the work to be completed for the thesis including improving the current modeling and analysis, exploring additional aspects and adding control in order to climb more complicated terrains.

Chapter 2

Related Work

This mechanism is unique but its underlying mechanisms draws from many areas including minimalist manipulation, walking and hopping robots, open-loop controlled robots and planning for dynamical system. These are briefly summarized in this chapter.

2.1 Minimalism

In the context of this work, the minimalist approach is the attempt to find the simplest mechanism that is capable of performing a given task. Simplicity of a system can be defined in different ways. In general one tries to minimize the amount of sensory input, actuation or computation. Previous minimalism works have dealt with manipulation and locomotion. Canny and Goldberg (1995) examined how a simple system comprising of a parallel-jaw gripper and an optical beam sensor, together with geometric planning and sensing algorithms is capable of recognizing and orienting a broad class of industrial parts. Erdmann and Mason built a tray-tilting system which can orient a part in a random initial configuration in the tray without sensing (Erdmann and Mason, 1988). Lynch and Mason (1999) planned and controlled dynamic nonprehensile manipulation. They used a one degree of freedom arm to perform dynamic tasks such as snatching an object from a table, rolling the object on the arm, and throwing and catching. A good example of minimalism

in the locomotion task is the passive dynamic walkers described below (McGeer, 1990a,b; Garcia et al., 1998).

The mechanism proposed in this work extends the minimalism in locomotion from horizontal motions to vertical, climbing motions. The mechanism is able to achieve a climbing task, albeit a simple one, without sensing and control, with a single actuator and a simple mechanical design.

2.2 Walking robots

McGeer, who initiated the work on passive dynamic walking (McGeer, 1990a,b) showed that a properly designed walking machine can walk down a gentle slope without any active control or energy input, other than potential energy from the slope. The mass and link length parameters can be chosen so that the natural dynamics of the walker enters a stable limit cycle from a basin-of-attraction of initial conditions. This principle has been used in the design of passive walkers with counter-swinging arms (Collins et al., 2001) and low-power walkers capable of walking over flat ground (Collins et al., 2005). I use a similar tactic in our mechanism but instead of using gravity as a "dumb" actuator, I use a fixed symmetric oscillation.

2.3 Hopping robots

Dynamic climbing is in many senses similar to dynamically locomoting robots in particular hopping, passive dynamic walking, and running robots. The work of Raibert was particularly influential, as it demonstrated that simple control laws could be used to stabilize hopping and control the running speed and direction of 2D and 3D single-leg hoppers (Raibert and Brown, 1984; Raibert et al., 1984). The single-leg systems also serve as models for runners with multiple legs (Raibert et al., 1986; Raibert, 1986). This work inspired detailed analysis of the nonlinear dynamics of a hopping robot (Vakakis et al., 1991; Koditschek and Bühler, 1991) and gymnastic maneuvers in both simulation (Berkemeier and Fearing, 1998; Mombaur et al., 2005a) and exper-

iments (Hodgins and Raibert, 1990). To improve the energy efficiency of a hopping robot, Brown and Zeglin introduced the BowLeg hopper, which can traverse a series of stepping stones (Brown and Zeglin, 1998; Zeglin and Brown, 1998) using a highly efficient bow-like spring.

2.4 Climbing mechanisms

2.4.1 Quasistatic climbers

One aspect of the proposed work that differs from the work described above is that locomotion occurs largely in the vertical direction. While a number of wheeled robots have been designed for locomotion in vertical pipes, the proposed work is more closely related to articulated (e.g., legged) climbing robots. Most such robots are quasistatic. The Alicia3 robot climbs walls by using pneumatic adhesion at one or more of three "cups" connected by two links (Longo and Muscato, 2006). The climbing robots of Shapiro et al. (2005) and Greenfield et al. (2005) climb by kinematic or quasistatic bracing between opposing walls. Bretl (2006) and Bevly et al. (2000) both use foot-hold based climbing strategies. Specifically, the four-limbed free-climbing LEMUR robot goes up climbing walls by choosing a sequence of hand-holds/footholds, as well as motions to those footholds, that keep the robot in static equilibrium at all times (Bretl, 2006). Gecko-inspired directional dry adhesives allow Stickybot to climb vertical, smooth surfaces such as glass (Kim et al., 2007), and the RiSE and SpinybotII robots climb soft or rough walls using spined feet to catch on asperities in the wall (Autumn et al., 2005; Kim et al., 2005). Fig. 2.1 presents some of these quasistatic climbing mechanisms.

2.4.2 Dynamic climbers

Unlike the quasistatic climber, only a few mechanisms have been proposed to achieve a vertical climbing task using dynamic motions. Clark et al. (2006; 2007) are in the process of making the clawed RISE and SpinyBot robots more dynamic. They analyzed and designed a cockroach

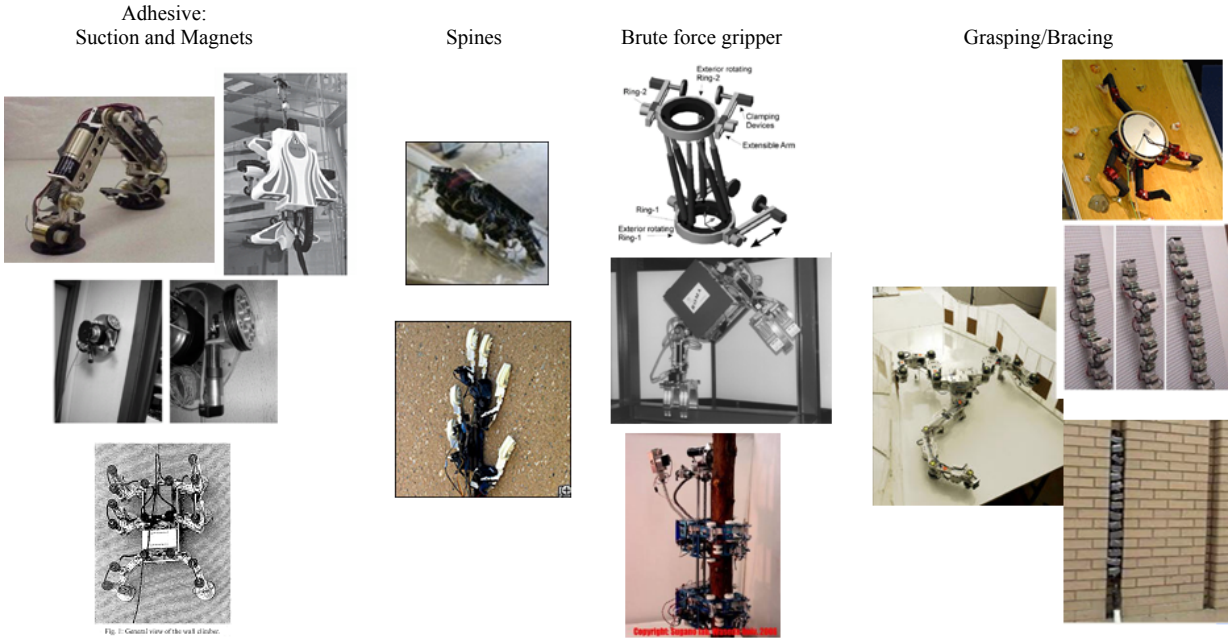

Figure 2.1: A few examples of quasistatic climbing mechanisms divided into four groups depending on the "attachment mechanism".

inspired dynamic climbing robot which resembles a biologically based template for dynamic vertical climbing. Their robot comprises a main rigid body with two linearly moving hands with springs. Two main differences sets the proposed DSAC apart from their dynamic climber. First, their mechanism is more complex in design since it uses two motors, energy storing springs, and a crank mechanism. Second, its climbing motion is similar to brachiating, flightless motion. During all times one arm is fixed to the ground. Lastly, in contrast to the proposed mechanism, the cockroach inspired robot does not use reaction forces from walls but rather uses spines to attach itself to a carpet covered wall.

2.5 Open-loop control

The classic control method of locomoting robots is feedback control, where the loop is closed in real-time using fast sensors and complicated feedback algorithms. For these reasons high on board computation is required and large amount sensory information. Ringrose (1997) and Mom-

baur et al. (2005a) have developed open-loop controls for dynamic hoppers. Ringrose (1997) used large circular feet to stabilize a one legged hopper. Mombaur and colleagues (Mombaur et al., 2005a,b) showed an approach which is similar to our proposed work. In this work one- and two-legged robots exhibit self-stabilizing running motions without closed-loop feedback. Two optimization loops are used: outer loop for finding stable motions by changing robot model parameters, such as length and masses, and an inner loop which searches for an optimal control by minimizing the control inputs under the robot constraints. I intend to adopt similar optimization techniques to find an optimal design and control of the DSAC for fast climbing.

2.6 Planning for dynamic systems

The broader goal of this thesis other than investigating the open-loop, simple, climbing mechanism is to use minimal information to try to traverse harder terrain. This requires some control and planning. Similar to the control of a hopping robot, or in our case a climbing robot, the task of juggling used simple planning and control. In all three cases, the primary purpose of the controller is to control the impact (or stance) event to achieve a desired limit cycle. To achieve stable juggling a few approaches were taken. As examples, Aboaf et al. (1989) used learning control, Lynch and Black (2001) used control based on gradient descent about a nominal batting trajectory, Ronsse et al. (2006) used control with minimum feedback (impact time only), and Bühler and Koditschek (1990), Rizzi and Koditschek (1992) introduced the "mirror law" control to juggle one or two objects in 2D and 3D.

Chapter 3

Background and Preliminaries

This chapter provides some background and preliminaries which will help to understand the following chapters. While it covers a wide array of topics this chapter is not intended to be a comprehensive explanation of all the concepts used in this manuscript. The chapter begins with the general formulation of the equations of motion of an articulated body together with added external forces. Nondimensionalizing equations of motion will finish this part of the chapter. Nonlinear dynamical systems definition and analysis methods conclude the chapter, including orbital stability, Poincaré maps, and bifurcations.

3.1 General Equations of Motion

3.1.1 Lagrangian formulation of equations of motion

The equations of motion differentially connect the input torques Υ and the resulting motion of the mechanism in state space. There are many ways to generate dynamic equations of motion of a mechanism. In this manuscript, the Lagrangian analysis is used to derive the equations of motion.

I use the classical definition of generalized coordinates, $q = (q_1, \ldots, q_n) \in Q$, of the mech-

anism as a minimal set of n independent coordinates which specifies the posture of the robot, where n is the number of degrees of freedom of the mechanism. This generalized coordinate vector contains joint angles and the cartesian location of one reference point on the robot relative to an inertial frame. The velocity vector $\dot{q} = (\dot{q}_1, \ldots, \dot{q}_n) \in T_qQ$ comprises both angular and linear velocities. The entire state, including configuration and velocities, is $z = (q, \dot{q}) \in TQ$.

In order to derive the equations of motion, the Lagrangian $L : TQ \rightarrow \mathbb{R}$ is defined for a mechanical system as the difference between the kinetic and potential energy of the system.

$$L(q, \dot{q}) = T(q, \dot{q}) - V(q),$$

where T is the kinetic energy and V is the potential energy of the system written in generalized coordinates.

Definition 3.1 (Lagrange's equations (Murray et al., 1994; Greenwood, 1997))**.** The equations of motion for a mechanical system with generalized coordinates $q \in \mathbb{R}^m$ and Lagrangian L are given by

$$\frac{d}{dt}\frac{\partial L}{\partial \dot{q}_i} - \frac{\partial L}{\partial q_i} = \Upsilon_i \quad i = 1, \ldots, m, \tag{3.1}$$

where Υ_i is the external force acting on the i^{th} generalized coordinate. These are the generalized forces.

If the i^{th} joint is passive the generalized force vanishes, i.e., $\Upsilon_i = 0$. It is sometimes convenient to rewrite Eq. 3.1 in matrix form

$$M(q)\ddot{q} + h(q, \dot{q}) = \Upsilon \tag{3.2}$$

where for an n degree of freedom robot, $M(q) \in \mathbb{R}^{n \times n}$ is the positive definite symmetric mass matrix, $h(q, \dot{q}) \in \mathbb{R}^{n \times 1}$ is a vector summarizing the influence of Coriolis, centrifugal, and gravitational forces, and $\Upsilon \in \mathbb{R}^{n \times 1}$ is a vector containing the generalized forces.

3.1.2 Lagrange's equations with contact forces

Like many other articulated locomoting mechanisms, our mechanism uses the contact with the walls to locomote. When the mechanism is in contact with an obstacle these contact forces can be easily incorporated into the Lagrange equations by formulating corresponding contact constraints. These constraints come from the assumption that no sliding occurs at the contact and therefore no work is done by the contact constraint forces. Note that the constraint itself is the fact that the velocity of the contact point itself is zero, not the work at that point. The contact constraints can be written as

$$A(q)\dot{q} = 0 \quad A(q) \in \mathbb{R}^{k \times n}. \tag{3.3}$$

where the constraint matrix A represents a set of k velocity constraints. In our kind of system, n is the number of degrees of freedom of the system and k is the number of constraint forces. When a system having a single unilateral constraint such as our mechanism hitting the wall, $k = 2$ which will include normal and tangential contact forces. This constraint matrix can be derived as $A(q) = \frac{\partial P(q)}{\partial q} \in \mathbb{R}^{2\times 3}$, where $P(q) = (P_x \quad P_y)^T$ is the point of contact with the walls. The dynamics of the system can now be written as

$$\frac{d}{dt}\frac{\partial L}{\partial \dot{q}} - \frac{\partial L}{\partial q} = \Upsilon_i - A^T(q)\lambda_{ext} \tag{3.4}$$

where λ_{ext} (the Lagrange multipliers) are the contact forces with the obstacle. Eq. 3.4 can be written in matrix form as

$$M(q)\ddot{q} + h(q,\dot{q}) = \Upsilon - A^T(q)\lambda_{ext} \tag{3.5}$$

By differentiating 3.3 and solving for $\ddot{q}$ from Eq. 3.5, the Lagrange multipliers are obtained

$$\lambda_{ext}(q,\dot{q}) = \left(A(q)M(q)^{-1}A(q)^T\right)^{-1}\left(\dot{A}(q)\dot{q} - A(q)M(q)^{-1}h(q,\dot{q})\right). \tag{3.6}$$

For a more careful derivation of these equations with constraints see the book by Murray et al. (1994).

3.1.3 State space representation

In many cases it is useful to transform the n second order differential equations into $2n$ first order differential equations which is also called state space representation. By first defining the state vector as $z = (q, \dot{q})^T$, the $2n$ first order differential equations are written as

$$\begin{aligned} \dot{z} = \begin{bmatrix} \dot{z}_1 \\ \dot{z}_2 \end{bmatrix} = \begin{bmatrix} \dot{q} \\ \ddot{q} \end{bmatrix} &= \begin{bmatrix} \dot{q} \\ M(q)^{-1}\left(\Upsilon - A^T(q)\lambda_{ext} - h(q,\dot{q})\right) \end{bmatrix} \\ &= \begin{bmatrix} z_2 \\ M(z_1)^{-1}\left(\Upsilon - A^T(z_1)\lambda_{ext} - h(z)\right) \end{bmatrix} \triangleq f(z, \Upsilon) \end{aligned} \tag{3.7}$$

3.1.4 Autonomous system vs. Non-Autonomous Systems

So far, the equations of motion were written as a system of equations

$$\dot{z} = f(z, \mu), \tag{3.8}$$

where $z = (q, \dot{q})$ is the state of the system. The parameters of the mechanism and the environment are denoted as μ. These parameters include the link lengths, masses, and the distance between walls. A system of ordinary differential equations is *autonomous* when it does not depend on time (or another independent variable). In contrast, a system is *non-autonomous* when it does depend on time. In 3.8, since the right hand side does not include time it is an autonomous system. A non-autonomous system is of the form

$$\dot{z} = f(z, t, \mu); \quad (z, t) \in \mathbb{R}^n \times \mathbb{R}, \tag{3.9}$$

A n$^{\text{th}}$-order time-periodic non-autonomous system with period T (i.e., $f(\cdot, t) = f(\cdot, t + T)$) can always be converted into an n+1$^{\text{th}}$-order autonomous system of differential equations (Guckenheimer and Holmes, 1983; Parker and Chua, 1989)

$$\begin{aligned} \dot{z} &= f(z, \tau, \mu), \\ \dot{\tau} &= 1; \quad (z, \tau) \in \mathbb{R}^n \times \mathbb{S}^1, \end{aligned} \tag{3.10}$$

where τ is the new state component representing time. The phase space has now been transformed into the manifold $\mathbb{R}^n \times \mathbb{S}^1$ (cylinder), where $\mathbb{S}^1 = \mathbb{R} \pmod T$ is the periodicity of the system. Note that for a periodic forcing of the shape $A\sin(\omega t)$, as in our system, another natural choice of the new state component can be $\tau = \omega t$, and therefore $\dot{\tau} = \omega$.

3.1.5 Nondimensionalizing Differential Equations

I propose to show that with a sinusoidal motor trajectory, and with the correct choice of parameters, the mechanism climbs stably. In order to reduce the dimension of the parameter space, I use a method called nondimensionalizing, or normalization. This method described in Appendix A can reduce the number of parameters by up to the number of fundamental units. In our system the number of parameters that can be reduced is three: mass, length, time. Instead of using the entire set of parameters, the idea of nondimensionalizing is to deal with ratios of these parameters. This will convert a system of differential equations into unitless (dimensionless) parameters. This method not only reduces the parameter space, but can also give intuitive and physically meaningful ratios of the parameters. For example, instead of looking at two masses of the system, the nondimensionalized parameter might be the ratio between the masses, or the ratio between one mass and the total mass of the system. Appendix A describes in detail the motivation and work flow of nondimensionalizing differential equations.

3.2 Nonlinear analysis

So far I have described the general formulation of the equations of motion for an articulated robot such as our climbing mechanism. The rest of this chapter deals with the methods used to analyze nonlinear dynamical systems. The section begins with an overview of orbital stability analysis and then describes more accurately how to use the Poincaré map to simplify the analysis of systems with limit cycles and finally describes a few nonlinear phenomena and the means to

interpret them.

3.2.1 Orbital stability - the Poincaré map

As mentioned previously, our system exhibits periodic motions due to the forced periodic constraint ($\phi(t)$). Moreover, the system is a *hybrid* system, one that cannot be described as a single continuous flow but only as a collection of continuous flows with discrete changes during the transitions. In our system, these discrete changes occur while impacting the walls. Due to these facts, a useful tool to analyze stability is the Poincaré map (Guckenheimer and Holmes, 1983). This tool converts the study of the hybrid periodic flow of our mechanism into a nonlinear discrete mapping on a lower dimensional space. By looking at the crossing of the flow with a cross section one can now analyze this discrete system instead of the more complicated hybrid flow. Period-1 motions, i.e., climbing motion which returns to its initial state after one period, will correspond to a single fixed point on the Poincaré section. Period-k motions, i.e., flow that returns to the same state after k periods, will correspond to k points on this section. The Poincaré map defined in this work, maps one state of the climbing robot, just after leaving the wall, to the state where the robot leaves the next wall. This is done by solving the equations of motion of the flight, impact, and stance phases numerically.

To find fixed points, I use the multidimensional Newton-Raphson numerical root finding method. To analyze the orbital stability, the Poincaré map is linearized around these fixed points. This linearization is the Jacobian at the fixed points. I find both stable and unstable fixed points. If the eigenvalues of this Jacobian are inside the unit circle then a perturbation from a limit cycle will converge to the unperturbed state, and this fixed point is said to be stable.

We now turn to more accurate definitions. As in Eq. 3.8, an autonomous differential equation can be described as

$$\dot{z} = f(z), \tag{3.11}$$

where $z \in \mathbb{R}^n$ is the state of the system and $f : \mathbb{R}^n \to \mathbb{R}^n$ is a Lipschitz-continuous vector field.

Thus, there exists exactly one solution for every initial condition $z(t_0) = z_0$. The solution is denoted by the trajectory $z(t)$ or by the flow $\Phi_t(z_0)$. The flow $\Phi_t(z_0)$ assigns a trajectory $z(t)$ to every initial value z_0.

Definition 3.2 (Periodic Solution, Periodic Orbit)**.** A solution $\Phi_t(z_0)$ of Eq. 3.11 is a periodic solution with period length $T > 0$ if $\Phi_{T+t}(z_0) = \Phi_t(z_0)$ holds for all times $t \in \mathbb{R}$.

The choice of z_0 is not unique; any point of the periodic solution is a valid starting value for an autonomous system.

Definition 3.3 (Poincaré map)**.** Consider an n-dimensional system as in 3.8. Let γ be a periodic orbit of some flow Φ_t in $\mathbb{R}^n$ arising from the nonlinear vector field $f(z)$. Let $\Sigma \subset \mathbb{R}^n$ be an $n-1$ dimensional cross section. The cross section Σ need not be planar, however, it must be transverse to the flow, i.e., all trajectories starting on Σ flow through it, not parallel to it. Denote the unique point where γ intersects Σ by p. Then the Poincaré map $\mathbf{P} : U \to \Sigma$ is defined in a neighborhood $U \subset \Sigma$ of p as

$$\mathbf{P}(q) = \Phi_\tau(q).$$

where $\tau = \tau(q)$ is the time taken for the orbit $\Phi_t(q)$ based at q to first return to Σ. If the mapping has a fixed point z^*, then $\mathbf{P}(z^*) = z^*$ (see Fig. 3.1). If multiple mapping is required for a state to return to itself, i.e.,

$$\mathbf{P}^k(z^*) = z^*,$$

the system has a period-k cycle, i.e., after k cycles that state maps back to the initial state. On the Poincaré section a period-k cycle will correspond to k points.

There are a few common types of Poincaré maps which differ by the chosen section. The two typical ones which are used in this analysis are the stroboscopic Poincaré map and the impact Poincaré map. The former is the more common map which takes the Poincaré section every equal time interval. The latter, which is commonly used in analyzing hybrid robotic systems, uses an event such as a leg of a robot hitting the floor as the Poincaré section.

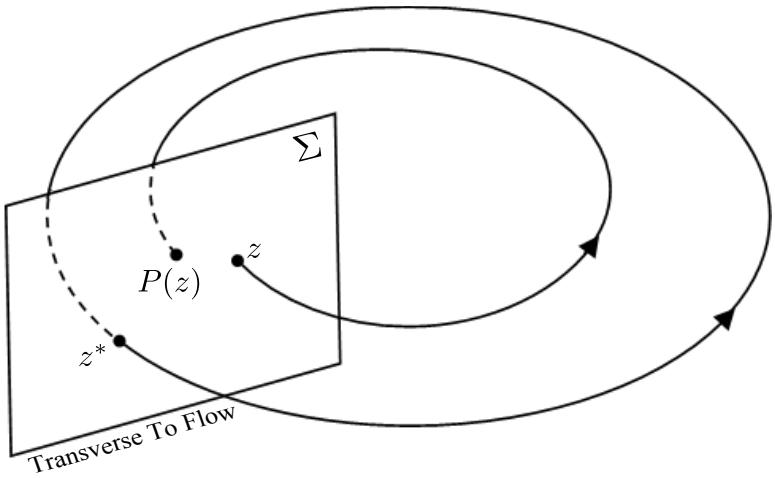

Figure 3.1: Poincaré map.

3.2.2 Stability definition

One of the most important and interesting questions asked when analyzing a dynamical system is whether the system is stable or not. Since our system is periodic, the orbital stability must be analyzed. As mentioned previously one can convert our system from a continuous or a hybrid system into a discrete system by using the Poincaré map method. Therefore instead of analyzing the stability of an orbit, the stability of a fixed point on the Poincaré section is analyzed. This fixed point corresponds to a closed orbit in the full state space. There are a few different forms of stability.

Definition 3.4 (Stable (Lyapunov Stable) Fixed Point)**.** A fixed point z^* of $f(z)$ is called stable if for any given neighborhood $U(z^*)$ there exists another neighborhood $V(z^*) \subseteq U(z^*)$ such that any solution starting in $V(z^*)$ remains in $U(z^*)$ for all $t \geq 0$.

Loosely speaking being Lyapunov stable means stability in the weak sense that trajectories starting nearby a limit cycle will remain nearby for all time. Asymptotic stability which is defined next also adds the constraint that at steady-state the flow is attracted back to the original limit cycle.

Definition 3.5 (Asymptotically Stable Fixed Point)**.** A fixed point z^* of $f(z)$ is called asymptot-

ically stable if it is stable and if there is a neighborhood $U(z^*)$ such that

$$\lim_{t\to\infty} |\Phi(t,z) - z^*| = 0 \quad \text{for all } z \in U(z^*)$$

In order to find if a fixed point of the Poincaré map is asymptotically stable Floquet analysis is used. Floquet analysis looks at the eigenvalues of the linearized map around the fixed point to determine its stability.

Theorem 3.1 (Characteristic (Floquet) Multipliers)**.** *Let z^* be a fixed point of the Poincaré map $\mathbf{P}$. The map $\mathbf{P}$ is n-dimensional for a non-autonomous systems and $n-1$-dimensional for an autonomous systems. The local behavior of the map near z^* is determined by linearizing the map at z^*. The linear map, called the Jacobian Matrix or the monodromy matrix, is*

$$\delta z_{k+1} = D\mathbf{P}(z^*)\delta z_k,$$

where δz_k and δz_{k+1} are a perturbation from the fixed point at iteration k and $k+1$, respectively. The eigenvalues of the Jacobian $D\mathbf{P}(z^*)$ are the characteristic multipliers of the periodic solution. These characteristic multipliers govern the evolution of perturbation δz_0 around the fixed point. (Parker and Chua, 1989; Nayfeh and Balachandran, 1995).

- *If all of the characteristic multipliers are within the unit circle, then the corresponding fixed point is asymptotically stable. Hence, the associated periodic orbit is asymptotically stable and is an attracting limit cycle. This fixed point is called an attractor.*
- *If all of the characteristic multipliers are outside the unit circle, the corresponding fixed point is unstable. Therefore, the associated periodic orbit is an unstable limit cycle. This fixed point is called a repellor.*
- *If some, but not all, of the characteristic multipliers are outside the unit circle, the corresponding fixed point is a saddle. Hence, the associated periodic orbit is an unstable limit cycle of the saddle type. See Fig. 3.2.*

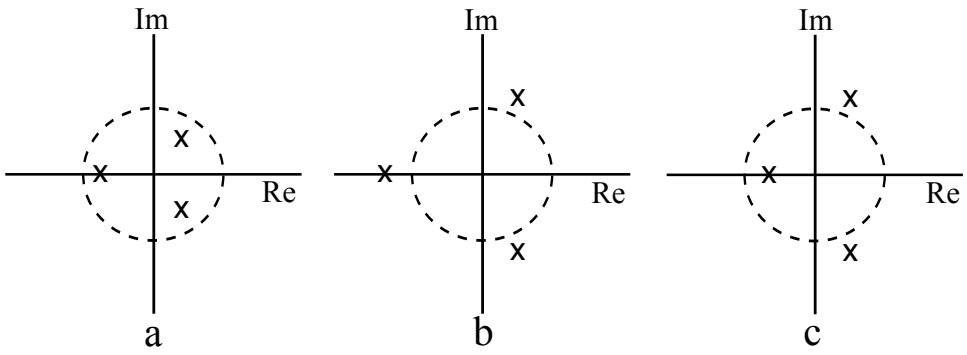

Figure 3.2: The position in the complex plane of the characteristic multipliers at a hyperbolic fixed point determines the stability of the fixed point. (a) asymptotically stable (b) unstable (c) non-stable, saddle type.

Note, this classification scheme remains valid as long as none of the characteristic multipliers lies on the unit circle. A fixed point with no characteristic multipliers on the unit circle is called hyperbolic. The stability of a non-hyperbolic fixed point cannot be determined from the characteristic multipliers alone unless one characteristic multiplier has magnitude greater than one and another characteristic multiplier has a magnitude less than one, in which case the fixed point is non-stable. To characterize non-hyperbolic fixed points, one must investigate the higher order nonlinear terms.

Proof. If one looks at the map of a perturbed state $z^* + \delta z_{k+1} = \mathbf{P}(z^* + \delta z_k)$, expanding the result in a Taylor series about z^* and retaining the linear terms, one obtains

$$z^* + \delta z_{k+1} = \mathbf{P}(z^* + \delta z_k) \approx \mathbf{P}(z^*) + D\mathbf{P}\delta z_k.$$

Therefore a perturbation from the fixed point decays if all the eigenvalues of DP are less than one. Hence, the system is locally stable around this linearization. The smaller the eigenvalue, the faster this perturbation decays. See (Nayfeh and Balachandran, 1995) or (Parker and Chua, 1989) for the full proof. □

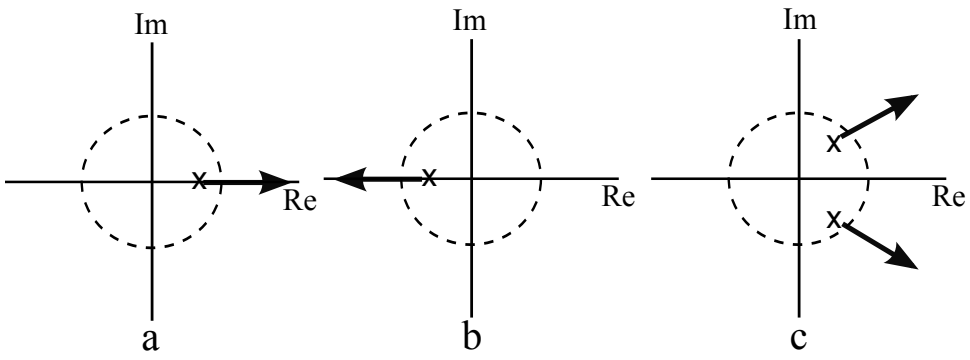

Figure 3.3: Scenarios depicting how the Floquet multipliers leave the unit circle for different local bifurcations: (a) transcritical, symmetry breaking, and cyclic-fold bifurcations; (b) period-doubling bifurcation; and (c) secondary Hopf or Neimark bifurcation. (Nayfeh and Balachandran, 1995)

3.2.3 Bifurcations of nonlinear systems

Definition 3.6 (Bifurcation)**.** Once again consider an n$^{\text{th}}$-order system

$$\dot{z} = f(z, \mu)$$

with a parameter $\mu \in \mathbb{R}$. As μ changes, the steady-state solution of the system also changes. If a small change in μ causes a steady-state solution to undergo a qualitative change it is called a bifurcation and the value at which a bifurcation occurs is called a bifurcation value (or point). Note that typically a small change in μ produces small quantitative changes in a steady-state solution. For instance, perturbing μ could change the position of a steady-state solution slightly, and if the steady-state solution is not an equilibrium point, its shape or size could also change.

The bifurcations can be analyzed using the characteristic multipliers defined in Definition 3.1. Three typical bifurcations related to the characteristic multipliers leaving the unit circle are shown in Fig. 3.3.

3.2.4 Types of dynamic motions

There are three classic types of dynamic motions which are relevant to our climbing mechanism:

- equilibrium (fixed point);
- periodic motion or a limit cycle;
- quasiperiodic motion which contains a finite number of incommensurable frequencies [1].

These motions are called attractors, because if some form of damping is present the transients decay and the system is "attracted" to one of the above three states.

The fourth kind of motion is called Chaos, which is associated with a "strange attractor". I will not go into details about this kind of motion, however I will try to define it in a simple manner and later show how to analyze and find chaotic motions. The main engineering motivation in searching for a chaotic region is to try to avoid these motions.

Definition 3.7 (Chaotic Motion)**.** Chaos is aperiodic long-term behavior in a deterministic system that exhibits sensitive dependence on initial conditions

Aperiodic long-term behavior means that the system does not reach a steady state solution of one of the above attractor solutions: equilibrium, periodic motion or quasiperiodic motion. A system is **deterministic** when the later states of the system follow from the earlier ones. In dynamical systems this implies that the system has no random or noisy inputs or parameters. **Sensitive** dependance to initial condition occurs when two very close initial conditions diverge exponentially from each other. In the next section I will briefly show a few methods to analyze periodic solutions and search for chaotic regions.

3.2.5 Methods of analyzing nonlinear systems

3.2.5.1 The Poincaré map

The most popular method to analyze periodic, forced systems is the Poincaré map which was previously discussed. By observing the crossing of the system through the Poincaré section, one can easily distinguish between different motions.

[1] Frequencies are incommensurable if their ratio cannot be expressed as a ratio of whole numbers.

- A k-periodic motion maps to k points on the Poincaré section, i.e., period-1 motion maps to a single point on the Poincaré section, period-2 motion maps to two points, etc.
- A quasiperiodic motion which contains a finite number of incommensurable frequencies traces a continuous closed curve on the Poincaré map since it does not converge to a single point.
- If the Poincaré map does not consist of either a finite set of points or a closed curve, the motion **may** be chaotic [2].

3.2.5.2 Lyapunov exponents

One of the important characteristics of chaos is sensitive dependance on initial conditions. The Lyapunov exponents can reveal if indeed there is an exponential relationship between the flow of two very close initial conditions. In general, for an n-dimensional dynamical system, there are n Lyapunov exponents. To check for sensitivity of initial conditions, only the largest Lyapunov exponents is of interest. The method for finding this largest Lyapunov exponent is very similar to finding the Lyapunov exponent of a one-dimensional map which is explained next.

Definition 3.8 (Lyapunov Exponents for 1-D maps)**.** Assume P is a Poincaré map of a 1-D system. Let z_0 and $z_0 + \Delta z_0$ be two nearby initial points on the flow, not necessarily in steady state. After one iteration of a map the points are separated by

$$\Delta z_1 = P(z_0 + \Delta z_0) - P(z_0) \simeq \Delta z_0 P'(z_0)$$

where $P' = dP/dz$. The local Lyapunov exponent λ at z_0 is

$$\lambda = ln|\frac{\Delta z_1}{\Delta z_0}| \simeq ln|P'(z_0)|$$

To obtain the global Lyapunov exponent, an average of the local Lyapunov exponent over many

[2]This only insures that this system does not have an aperiodic behavior but not necessarily sensitivity to initial conditions.

iterations must be taken

$$\lambda = \lim_{N\to\infty} \frac{1}{N} \ln |\frac{\Delta z_1}{\Delta z_0}|. \tag{3.12}$$

This is similar to calculating the eigenvalues of the linearized Poincaré map. In fact, the Lyapunov exponents for higher dimensional systems can also be calculated as the average moduli of the eigenvalues

$$\lambda_i = \lim_{t\to\infty} \frac{1}{T} \ln |m_i(T)|.$$

where $m_1, m_2 \ldots m_n$ are the eigenvalues of $DP(z)$.

The Lyapunov exponents are closely related to the eigenvalues discussed previously and are calculated by similar means, but there is an important difference. Whereas eigenvalues are usually calculated at a point in state space, such as a fixed point, Lyapunov exponents are usually geometrically averaged along the orbit. The Lyapunov exponents are the average rate of contraction or expansion near the periodic orbit. Knowing how the local Lyapunov exponent varies in space allows one to identify regions of an attractor with good or poor predictability for small initial errors. More about numerical calculations of the Lyapunov exponents can be found in (Parker and Chua, 1989; Sprott, 2003).

3.2.5.3 Spectrum analysis - Fourier analysis

Another important tool in trying to diagnose a bifurcating nonlinear system is the power spectrum analysis. This method studies the frequency content of a solution of a nonlinear ODE. By first taking the time series data and analyzing using fast Fourier transforms (FFT), one can find the dominant frequencies contained in the solution. A period-1 orbit will consist of the fundamental frequency and higher harmonic frequencies in multiples of the fundamental frequency. After a period doubling bifurcation occurs another frequency will join the fundamental one. This frequency will be half the frequency of the fundamental one. After each doubling bifurcation another frequency, and its corresponding harmonics, will join the spectrum.

Chapter 4

Preliminary Results

The work to date includes modeling the motion and the nonlinear dynamics of the dynamic climber and analyzing the stability bifurcation with change of parameters. As mentioned previously the broader scope of this work is to first analyze in depth the minimalist open-loop climber and then add some complexity in sensing in order to traverse harder, piecewise linear walls. The work in this chapter explores the work to date and shows a few proof-of-concept results and experiments.

4.1 Modeling

4.1.1 System description and modeling assumptions

In simulations and experiments this system exhibits stable periodic climbing motions. The goal of our analysis is to produce a model which exhibits behavior similar to that of the experiments and simulations. The proposed mechanism is planar and consists of two links; the first is the main body and the second is the leg which is connected to the main body through an actuated revolute joint and contacts the wall (Fig. 4.1). For simplicity, the inertial frame is chosen on the symmetric line half of the distance between the two parallel walls. A few hypotheses and

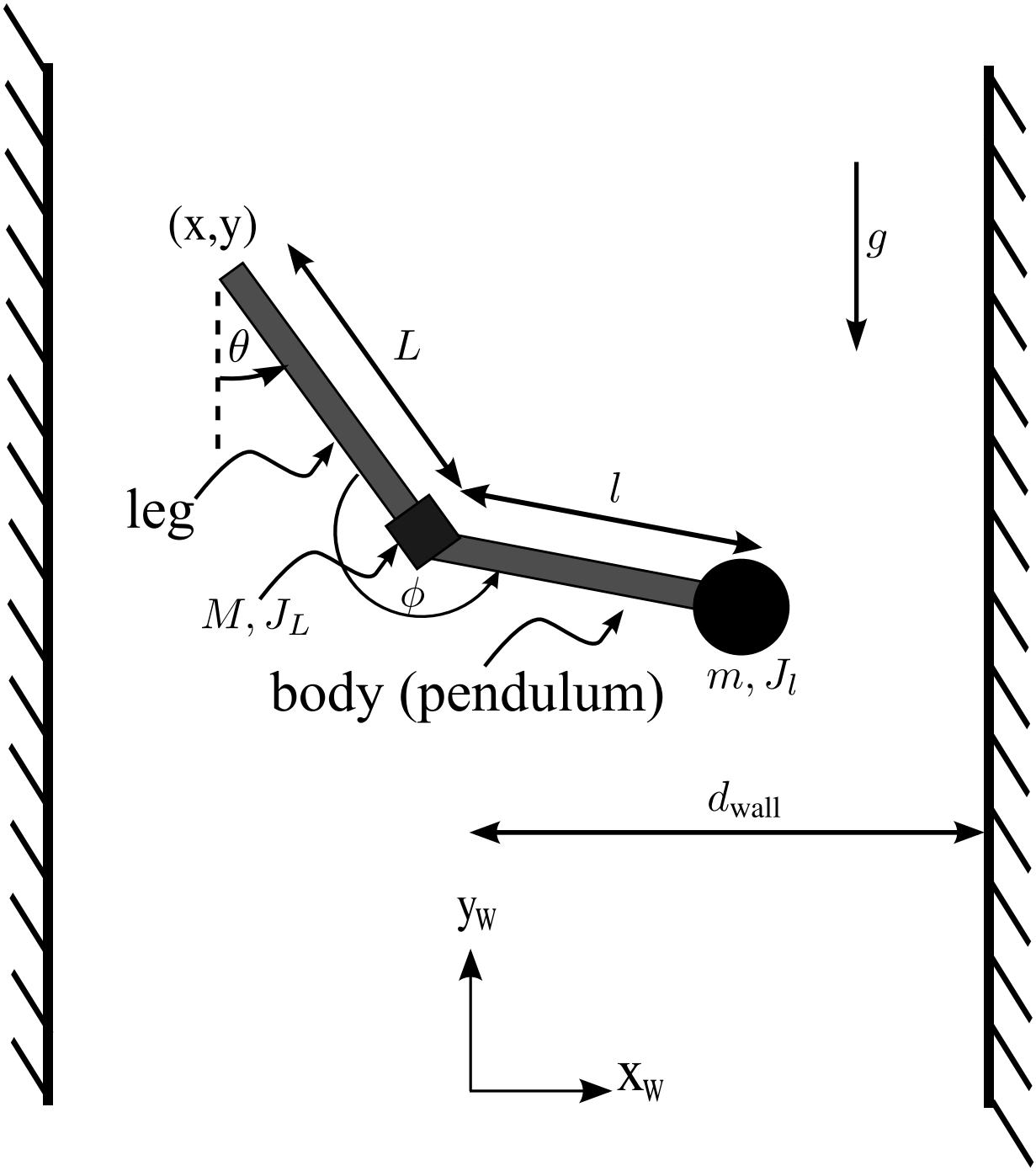

Figure 4.1: Schematics of two link mechanism climbing between two parallel walls.

assumptions are used throughout in order to simplify the analysis. I will now enumerate them together with the modeling characteristics:

1. The **leg** is assumed be very thin with mass M concentrated at the end of the leg (location of the actuated joint), moment of inertia J_L and total length L. Only the leg contacts the walls.

2. The **body** is assumed be very thin with a point mass m concentrated at the end of the body, moment of inertia $J_l = 0$, and total length l. The body does not collide with the leg nor with the walls.

3. The **actuation** is achieved through a high gear ratio motor which is assumed to achieve a known trajectory $\phi(t) = A\sin(\omega t)$.

4. The **gait** of the system consists of three phases:

   (a) Flight phase: during this phase there is no contact between the walls and the leg.

   (b) Impact phase: this is the instantaneous phase where the leg hits the walls.

   (c) Stance phase: during this phase the leg is in contact with the wall. We consider only the gait where the distal end of the leg hits the wall. Due to high friction between the leg and the wall, and point contact during the stance phase the contact is treated as a frictionless pin joint.

5. **Impact** of the leg with the wall is assumed to be instantaneous, fully plastic (inelastic) and without sliding.

   From these assumptions we can infer that

   (a) the configuration of the point of contact does not change and the velocity of the point vanishes.

   (b) Since the motor has a high gear ratio and has a known trajectory, during the impact the motor can apply a high torque to keep itself on track.

   (c) The angular momentum around the contact point is conserved.

All the analytical calculations for deriving the equations of motion were done in Mathematica™, while numerical calculations were done in Matlab™. In the proposed work I intend to generalize this model from point masses to a more realistic models adding the location of COM and adding inertia to the body.

4.1.2 General equations of motion

Since our system includes a periodic forced input, as discussed in Chapter 3, Eq. 3.9, we can describe the system as an non-autonomous system

$$\dot{z} = f(z, t, \mu), \tag{4.1}$$

where $z = (q, \dot{q})$ is the state of the system. The generalized coordinates are denoted as $q = (x, y, \theta, \phi) \in \mathbb{R}^2 \times \mathbb{S}^1 \times \mathbb{S}^1$. As depicted in Fig. 4.1, x and y are the coordinates of the end of the leg, θ is the angle between the vertical and the leg, and ϕ is the angle between the leg and the body. The parameters of the mechanisms and the environment are denoted as μ. These parameters include, for example, the link lengths and the distance between walls. In our system I assume that the angle ϕ has a constrained motion. Specifically, it is a symmetric sinusoidal of the form

$$\phi(t) = A \sin(\omega t), \tag{4.2}$$

where A and ω are the amplitude and angular frequency of the sinusoid, respectively. Since ϕ is a constrained motion, there is no need to include ϕ and $\dot{\phi}$ in the state, hence we can write the system as an autonomous system similar to Eq. 3.8

$$\dot{z} = f(z, \mu), \tag{4.3}$$

The state z is $(q, \dot{q})$, where $q = (x, y, \theta, \tau) \in \mathbb{R}^2 \times \mathbb{S}^1 \times \mathbb{S}^1$, $\tau = \omega t \pmod{2\pi} \in \mathbb{S}^1$, and $\dot{q} = (\dot{x}, \dot{y}, \dot{\theta}, \omega)$. Writing in Lagrange matrix form, as in Eq. 3.5, the equations of motion are

$$M(q)\ddot{q} + h(q, \dot{q}) = \Upsilon - A^T(q)\lambda_{ext}, \tag{4.4}$$

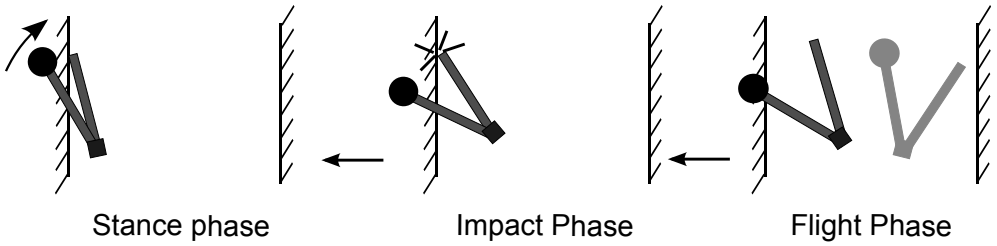

Figure 4.2: Three phases of climbing gait.

where $M(q) \in \mathbb{R}^{3\times3}$ and $h(q,\dot{q}) \in \mathbb{R}^{3\times1}$ are the mass matrix and the nonlinear terms matrix, respectively. The vector representing the applied forces and torques is $\Upsilon \in \mathbb{R}^{3\times1}$ and λ_{ext} is the contact force with the wall. Since ϕ is a constrained motion there is no need to include input torques (Υ). Let $A(q) = \frac{\partial P(q)}{\partial q} \in \mathbb{R}^{2\times3}$ be the constraint matrix during contact, where $P(q) = [P_x \quad P_y]^T$ is the point of contact with the walls. Since the point of contact $P(q)$ coincides with our coordinate system, $P(q) = [x \quad y]^T$ and $A(q) = \left(\begin{smallmatrix} 1 & 0 & 0 \\ 0 & 1 & 0 \end{smallmatrix}\right)$. This system is underactuated in the sense that only one actuator exists. This is the motor which connects the leg to the main body. For a detailed derivation of these equations of motion see Appendix B.

As mentioned before, to analyze the behavior of the mechanism, the motion is split into three phases: flight, impact, and stance phase (see Fig. 4.2). By using the final state of one phase as the initial values of the next phase we can analyze and simulate the whole climbing motion.

A projection of the phase space portrait, including only θ and $\dot{\theta}$ of a climbing gait from one wall to the other and back to the first, is depicted in Fig. 4.3. This motion consists of two consecutive three-phase motions which will now be derived in more detail.

4.1.2.1 Free flight phase

During free flight, there are no external forces acting on the mechanism other than gravity. Therefore, $\lambda_{ext} = 0$ and the equations of motion are reduced to:

$$M(q)\ddot{q} + h(q,\dot{q}) = 0, \tag{4.5}$$

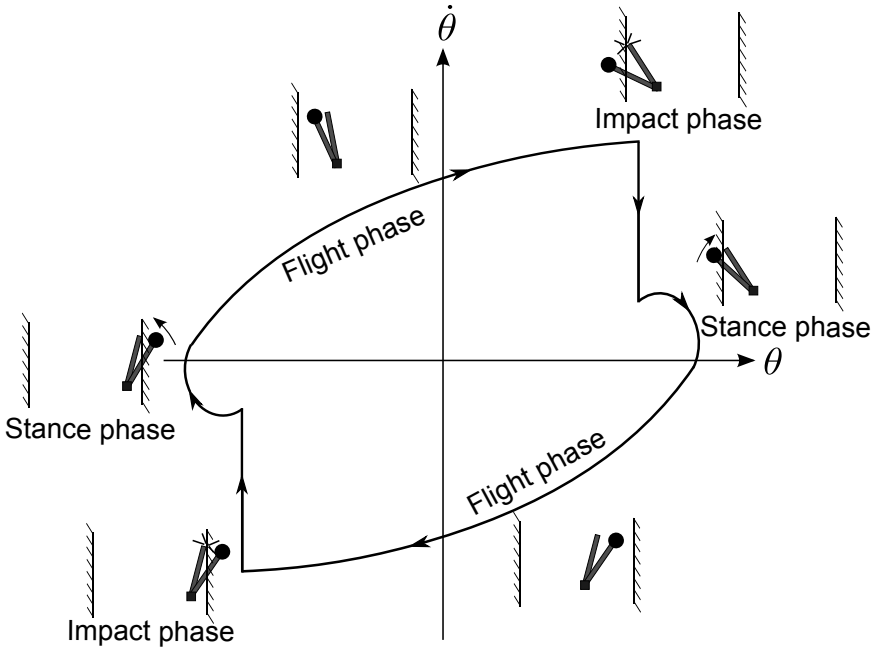

Figure 4.3: phase plot of a typical climbing motion.

4.1.2.2 Impact phase

From the impact assumptions which were proposed in sec. 4.1.1 one can find the equation of conservation of angular momentum around the contact point during the instantaneous time of impact. As described in (Greenwood, 1997), the total angular momentum with respect to point c is

$$H = \sum_{i=1}^{N} I_i \omega_i + r_{m_i/c} \times m_i \dot{r}_{m_i}, \tag{4.6}$$

where N is the number of links, $r_{m_i/c}$ is the vector from mass i to the point of contact. $\dot{r}_{m_i}$ is the velocity of mass i relative to the inertial frame. I_i is the moment of inertia of link i and ω_i is the angular velocity of link i as depicted in Fig. 4.4.

From the previous assumptions we know that during impact, only the velocity and not the configuration changes, hence the only unknown state variable is $\dot{\theta}$. From this equation we can find the new $\dot{\theta}^+$ after the collision. This is done by equating the angular momentum before impact and instantaneously after impact.

$$\dot{\theta}^+ = f(\theta, \phi, \dot{x}^-, \dot{y}^-, \dot{\theta}^-), \tag{4.7}$$

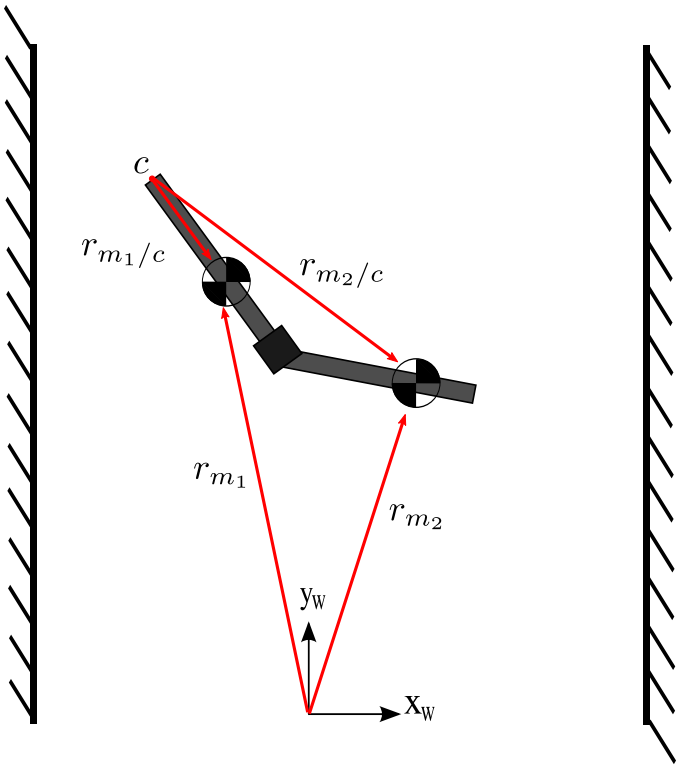

Figure 4.4: Finding angular momentum around contact point c.

where f maps the angular velocity of the leg from pre-impact to post-impact.

Since the environment is symmetric (two parallel walls), we can include a "flip" of coordinates during impact phase, this will enable the equations to always represent a robot leaping off the right towards the left wall. All of the state coordinates other than the y coordinates will change sign. Since, by assumption, no sliding is allowed, the linear velocities will vanish after

impact. Therefore there exists a mapping which describes this whole transition during impact

$$\begin{bmatrix} x^+ \\ y^+ \\ \theta^+ \\ \phi^+ \\ \dot{x}^+ \\ \dot{y}^+ \\ \dot{\theta}^+ \\ \dot{\phi}^+ \end{bmatrix} = \begin{bmatrix} -x^- \\ y^- \\ -\theta^- \\ -\phi^- \\ 0 \\ 0 \\ -f(\theta, \phi, \dot{x}^-, \dot{y}^-, \dot{\theta}^-) \\ -\dot{\phi}^- \end{bmatrix}, \tag{4.8}$$

where the $^-$ and $^+$ subscripts represent the pre and post impact state variables, respectively.

4.1.2.3 Stance phase

Since I assume that the leg which is in contact with the wall will not slip, the external (contact) force can be added and the system can be described as

$$M(q)\ddot{q} + h(q, \dot{q}) - A^T(q)\lambda_{ext} = 0, \tag{4.9}$$

where $\lambda_{ext} = [\lambda_n, \lambda_t]^T$ are the normal and tangential contact forces between the tip of the leg and the wall. As described in Eq. 4.4, the constraint matrix $A(q)$ is $A(q) = \left(\begin{smallmatrix} 1 & 0 & 0 \\ 0 & 1 & 0 \end{smallmatrix}\right)$. We add an extra set of equations to find the time when the normal contact force changes sign. This is the instant when the leg looses contact with the wall and the mechanism transitions into flight phase. As shown in section 3.1.2, we can apply some simple manipulation to add the Lagrange multiplier constraint and find the external force equation as a function of the state.

$$\lambda_{ext}(q, \dot{q}) = \left(A(q)M(q)^{-1}A(q)^T\right)^{-1}\left(\dot{A}(q)\dot{q} - A(q)M(q)^{-1}h(q, \dot{q})\right). \tag{4.10}$$

When λ_n changes sign, the stance phase terminates and the flight phase begins. Using the final conditions of the stance phase as the initial conditions of the flight phase, we can continue and simulate the next three phases. The three phases including the flip during impact phase are shown in Fig. 4.5.

4.1.2.4 Summary of modeling

Thus far I have shown how the climbing motion of the proposed mechanism can be decomposed into the three phases. The impact phase also includes a "flip" which essentially allows us to always analyze a leap from the right wall to the left wall. The full derivation of these three phases is provided in Appendix B. As previously mentioned, instead of using the parameters of the mechanism, it is possible to convert the equations of motion into nondimensional equations. The nondimensional parameters, which are not a necessarily unique, are extracted. The nondimensional parameters are

$$m^* = \frac{m}{m+M}, \quad l^* = \frac{l}{L}, \quad L^* = \frac{L}{d_{wall}}, \quad J_L^* = \frac{J_L}{L^2(m+M)}, \quad \gamma = \frac{g}{d_{wall}\omega^2}, \quad A. \tag{4.11}$$

These nondimensional parameters provide some valuable information without even observing or solving the equations of motion. These are the important ratios of the system.

4.2 Analysis

4.2.1 A typical climbing motion

Figure 4.3 depicted a full climbing cycle between one wall to the other and back to the first. Figure 4.6 depicts a typical period-1 phase plot cycle for the new climbing motion after adding the "flip", as in Eq. 4.8. This plot is a phase plot of θ and $\dot{\theta}$. Although this is not the full state space but only a projection on the $\theta, \dot{\theta}$ plane, this phase plot portrays the important information of

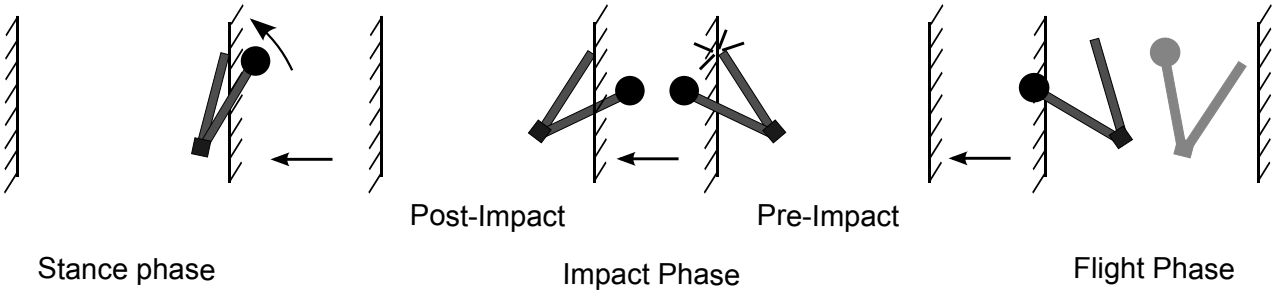

Figure 4.5: Three phases including flip during impact phase.

the climbing cycle. In fact, I will later show that these two state variables together with a variable corresponding to phase are all the information needed to portray the motion of the mechanism.

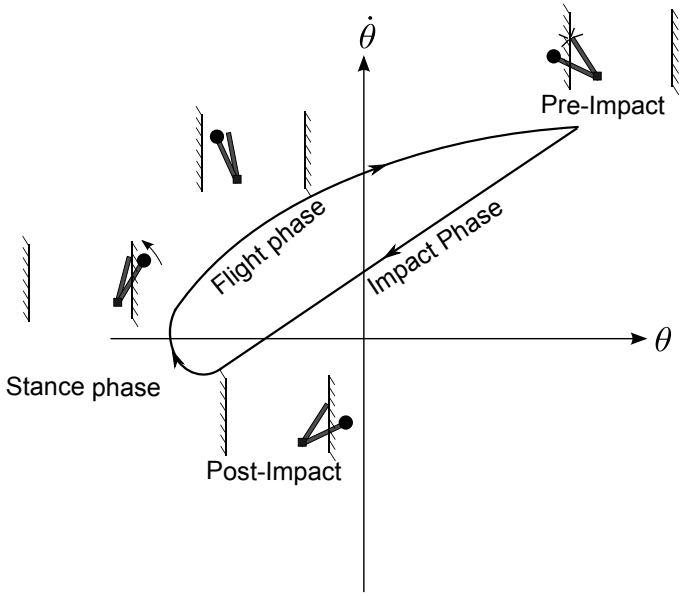

Figure 4.6: phase plot of a typical climbing motion with the flipping action of impact phase.

4.2.2 Open loop stability

This section explains the stability investigation of the climbing mechanism. There are several approaches to investigate nonlinear systems. One, which for example was taken by McGeer (1990b), is to linearize the governing equations of motion about an equilibrium state. This might allow us to explicitly integrate the equations of motion. There are two problems with this approach. The first is that the solutions are only valid in a small region around the linearized state. This accounts for the loss of important information and for inaccurate stability models (as shown in Goswami et al., 1998). The second problem is that in our mechanism, in order to calculate the time of flight, a transcendental equation must be solved. This forces us to solve the equation numerically. The second approach, which is used here, is to preserve the full, nonlinear hybrid equations of the system. The main disadvantage in this approach is that we must rely on numerical solutions.

Using the definitions of orbital stability from Sec. 3.2.1, I will explore the regions where the

mechanism is stable. One should note that we are only interested in the orbital stability, i.e., the stability related to a closed orbit (or limit cycle). Similar to other locomoting systems, one state variable is related to the progression of the mechanism. In walking machines this is the horizontal coordinate, whereas in our system it is the vertical displacement (y). Since our system locomotes, this variable is not cyclic hence we are not interested in finding its orbital stability. One might either ignore this variable, as done in most related work, or show that the equations of motion are invariant to this variable, therefore will not be cyclic in general. The next theorem will explain why invariance of the displacement variable corresponds to a non-cyclic motion.

Theorem 4.1. *Consider an n dimensional system of ODE with state $\{z_1, z_2, \ldots, z_{2n}\}$. If the system is invariant to one of the generalized coordinates, i.e., $\dot{z} = f(z_2, z_3, \ldots, z_{2n})$, then*

1. *The system can be solved by first solving the reduced $n-1$ dimensional system $\dot{\zeta} = f(\zeta)$, where $\zeta = (z_2, z_3, \ldots, z_{2n})$, followed by solving the single ODE $\dot{z}_1 = f(\zeta)$.*
2. *The invariant variable z_1 can never be a non zero-mean periodic on average, I.e., on average the variable will either increase or decrease.*

Proof. The sketch of the proof is straightforward. Since the system is invariant to z_1, it is possible to decouple the system into a reduced $n-1$ second order differential equations together with a single first order differential equations by substituting $u = \dot{z_1}$. This process is similar to reduction of order of a differential equation when a dependent variable is missing (e.g., Boyce and DiPrima, 2001). Second, after solving the reduced system, numerically in our case, one can simply integrate u to find z_1. The consequence of integrating $\dot{z}_1$ is that unless $\dot{z}_1$ has a zero mean z_1 will always either increase or decrease, hence will not be cyclic. □

Theorem 4.1 is significant to our system because our equations of motion are not dependent on the vertical displacement (y). Physically, since the walls are vertical, placing the robot in a different y location should not change the dynamics of the system other than initial condition. Moreover, since the robot climbs it does not make sense to find the orbital stability in that direction because it is not periodic. Therefore, the entire state space can be decomposed into two

spaces, the y climbing and the rest of the state which can be periodic and stable. For stability analysis we can use Theorem 4.1 and exclude the y variable. We will only use y when we are interested in finding how much the robot climbed.

We will now use the definitions of the Poincaré map outlined in the previous chapter to explore the local stability of the mechanism.

4.2.3 Poincaré map and corresponding Poincaré section

Using Definition 3.3, we can define the Poincaré map from the Poincaré section mapped back to this section by $\mathbf{P}$

$$z_{k+1} = \mathbf{P}(z_k), \tag{4.12}$$

where $\mathbf{P}$ is the map, z_k and z_{k+1} are the reduced spaces on the Poincaré section before and after the map, respectively. The dimension of reduced space on the Poincaré section can be extremely small if the section is chosen wisely. A convenient section to choose as the Poincaré section is the instant of release from the wall, i.e., the transition from stance to flight phase. This occurs when the normal contact force λ_n changes sign from negative to positive. Because during stance phase the end of the leg is touching the wall ($x = d_{wall}$), no rebound ($\dot{x} = 0$) or slippage ($\dot{y} = 0$) occurs , we can define a reduced dimensional hyperplane Σ as the Poincaré section

$$\Sigma = \{(x, \theta, \dot{x}, \dot{y}, \dot{\theta}, \tau) \in \mathbb{R}^4 \times \mathbb{S}^1 \times \mathbb{S}^1 \mid x = d_{wall}, \dot{x} = 0, \dot{y} = 0, \lambda_n(z, \tau) = 0\} \tag{4.13}$$

If the mechanism reaches the wall during the climbing cycle, then the state z must lie on Σ. Other motions which do not reach the wall cannot be analyzed using this method, however, they are not of interest since pushing off the wall is needed for stable climbing. Note that I did not include y in the definition of the Poincaré section because, as shown in Theorem 4.1, y is not periodic hence not relevant to the orbital stability analysis. All of these Poincaré section constraints reduce the state of this section to three: θ, $\dot{\theta}$, and τ. The last state variable (phase) comes from the conversion to an autonomous system which corresponds to the state of the pendulum relative to the leg.

Although this Poincaré section reduces the state tremendously (from eight to three) it is not trivial to calculate the exact transition, since the contact forces need to be calculated. I intend to use this full definition of the section in my future thesis work, however, in this proposal I simplify the section even further by assuming that the transition between stance and flight phases occurs when the acceleration of the swinging leg (ϕ) changes sign, i.e., when $\ddot{\phi} = -A\omega^2 \sin(\omega) = 0$. This event occurs when $\tau = \omega t \pmod{2\pi} = 2\pi$. This assumption is nearly correct in most climbing scenarios. Nonetheless, I will try to omit this assumption in the future thesis analysis. By using this simplification, instead of calculating the forces in stance phase and finding the event when the normal force change sign, we can define the Poincaré section when $\tau = 2\pi$. The new Poincaré section can therefore be defined as

$$\Sigma = \{(x, \theta, \dot{x}, \dot{y}, \dot{\theta}, \tau) \in \mathbb{R}^4 \times \mathbb{S}^1 \times \mathbb{S}^1 \mid x = d_{wall}, \dot{x} = 0, \dot{y} = 0, \tau = 2\pi\} \tag{4.14}$$

In this Poincaré section all state variables are constrained, except θ and $\dot{\theta}$. Therefore, the Poincaré map is defined as

$$\mathbf{P} : \mathbb{S}^1 \times \mathbb{R} \rightarrow \mathbb{S}^1 \times \mathbb{R},$$

including only $\theta, \dot{\theta}$.

4.2.4 Local stability

As mentioned previously, stability of the climbing mechanism refers to local orbital stability, i.e., the stability of an orbit in phase space around a fixed point. In order to find this kind of stability we must first find the fixed point of the Poincaré map, then linearize the Poincaré map around the fixed point, and finally find the eigenvalues of this linearized Poincaré map. This investigation is conducted numerically by first using the Newton-Raphson method to find the fixed point, and then calculating the Jacobian (linearized Poincaré map) and its eigenvalues numerically.

4.2.4.1 Fixed point search

The fixed point is the initial state of the mechanism that will map back to itself after one Poincaré map. Thus, we need to solve the equation

$$\mathbf{F}(z) \triangleq z - \mathbf{P}(z) = 0. \tag{4.15}$$

This search is done by fixing the mechanism parameters and using the multidimensional Newton-Raphson method to search for the state space that will map back to itself. The solution is not guaranteed and may not be unique. Note that during the Newton-Raphson search we need to solve Poincaré map, i.e., forward simulate the three phases. During the flight phase, if the mechanisms does not reach the wall after a certain integration time it is concluded that there is no fixed point. In fact, even if there is a fixed point, it will not be of interest for our climbing analysis because it will likely not be climbing at all.

4.2.4.2 Linearized Poincaré map and eigenvalues

The linearized Poincaré map around the fixed point that was previously found, is the Jacobian of the map

$$\nabla \mathbf{P} = \begin{bmatrix} \dfrac{\partial \mathbf{P}}{\partial \theta} & \dfrac{\partial \mathbf{P}}{\partial \dot{\theta}} \end{bmatrix}^T. \tag{4.16}$$

Calculating the elements of the Jacobian is done numerically using either the central difference or the forward difference derivative approximation. The central difference can be slightly more accurate but requires more evaluations of the Poincaré map $\mathbf{P}$. Therefore, the simplified forward difference was chosen, which finds the elements of the Jacobian by perturbing the state by a small scalar dz in direction i, mapping $\mathbf{P}(z_1, \ldots, z_i + dz, \ldots, z_n)$, finding the difference between it and the unperturbed map, and finally taking the ratio to the perturbed amount. The i$^{\text{th}}$ element will therefore be

$$\frac{\partial \mathbf{P}}{\partial z_i} = \frac{\mathbf{P}(z_1, \ldots, z_i + dz, \ldots, z_n) - \mathbf{P}(z)}{dz} \tag{4.17}$$

for our system the Jacobian will be

$$\nabla \mathbf{P} = \begin{bmatrix} \dfrac{\mathbf{P}(\theta + dz, \dot{\theta}) - \mathbf{P}(\theta, \dot{\theta})}{dz} & \dfrac{\mathbf{P}(\theta, \dot{\theta} + dz) - \mathbf{P}(\theta, \dot{\theta})}{dz} \end{bmatrix}^T \tag{4.18}$$

The mapping $\mathbf{P}$ is stable if the Poincaré map of a perturbed state is closer to the fixed point. This property can be viewed as the contraction of the phase space around the limit cycle. This means that the magnitude of the eigenvalues of $\mathbf{P}$ at the fixed point are strictly less than one, as discussed in Chapter 3. The eigenvalue calculations were done using Matlab™.

4.3 Analysis results

Using the analysis process described in the previous sections I will explore the orbital stability characteristics of a typical DSAC mechanism. This analysis is further elaborated in the thesis work. The results given here are proof-of-concept examples of interesting phenomena and are not comprehensive. The results shown here are for the mechanism and environment parameters given in Table 4.1. Notice that the effective gravity is a tenth of the normal gravity. This will later help us in the experimental section to obtain interesting climbing phenomena using slower motor speeds.

4.3.1 Local stability - varying frequency and amplitude

Figure 4.7 shows the stability plot of the specific mechanism with parameters from Table 4.1 while varying ω and A. This plot is obtained by finding fixed points, linearizing around them and using the eigenvalues to check if a stable orbit exists. This plot reveals three important regions. The first is the region where no fixed point was found (Fig. 4.7- bottom left region). This does not mean that there is necessarily no fixed point, just that the integration was stopped after a certain amount of time during which the mechanism did not reach the opposite wall. The central region is the period-1 stable region. This area is where the climbing gait is a symmetric, stable period-1. The third region depicts the period-1 non stable together with the period-2 stable (Fig. 4.7- top

Table 4.1: Nondimensional parameters for results section.

Parameter[a]	Description	Value
m^*	Mass ratio $\frac{m}{m+M}$	0.7
l^*	Link length ratio $\frac{l}{L}$	$0.8^\dagger$
L^*	Link to walls gap ratio $\frac{L}{d_{wall}}$	$1\frac{2}{3}$
J_L^*	Nondimensional inertia $\frac{J_L}{L^2(m+M)}$	0.00355
γ	Nondimensional gravity $\frac{g}{d_{wall}\omega^2}$	$0.03486^\dagger$
A	Amplitude	$0.8^\dagger$
Parameters marked with † are varied in the current analysis		

[a]To obtain these nondimensional parameters these parameters can be used: M=0.3 Kg, m=0.7 Kg, L=0.075 m, l=0.06 m, $J_L = 2 \cdot 10^{-5}$ Kg m^2, ω=25 $\frac{\text{rad}}{\text{sec}}$, g=0.98 $\frac{\text{m}}{\text{sec}^2}$, d_{wall}=0.045 m

right region). The fixed point search found two fixed points, one that maps back to itself (period-1) and another that maps back to itself only after two cycles (period-2). The period-1 was found to be unstable whereas the period-2 is stable.

4.3.1.1 Bifurcations

The critical point where a change in stability between the stable period-1 and a stable period-2 orbit occurs is a bifurcation point as defined in Chapter 3. One way to nicely show these bifurcations is to take a slice from the stability plot (Fig. 4.7) while keeping one variable constant. For example, we can fix the amplitude to be $A = 0.8$ while varying the angular frequency ω and plotting one of the state variables. A bifurcation plot for ω vs. θ is presented in Fig. 4.8. This bifurcation plot clearly shows the first period doubling at around $\omega \approx 25\frac{\text{rad}}{\text{sec}}$. This is where a period-1 switches to a non-stable orbit while a new, stable period-2 is born. This plot is obtained by forward simulating the Poincaré map a few thousand cycles and plotting the resulting variables. Because this is a forward simulation, we cannot find the unstable (period-1 cycle) as was

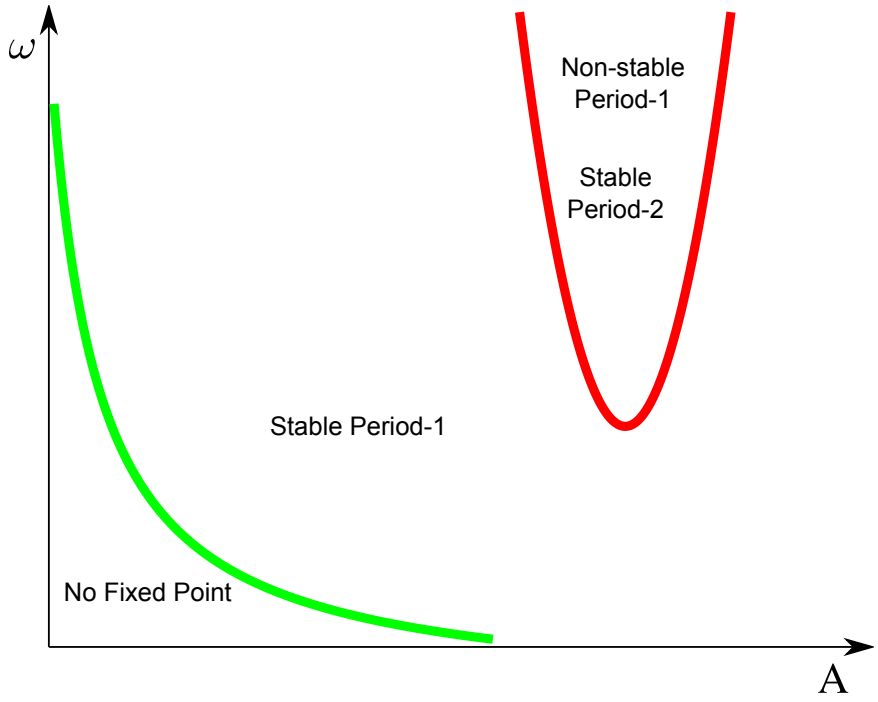

Figure 4.7: A-ω stability plot.

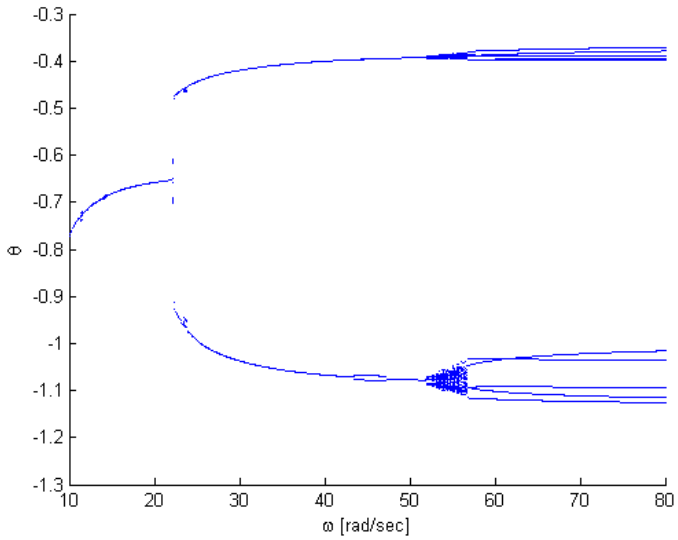

Figure 4.8: Bifurcation diagram.

found in the previous stability plot.

4.3.1.2 Power spectrum analysis

I use the power spectrum analysis tool which was briefly described in Chapter 3 to further analyze the bifurcation plot (Fig. 4.8). The power spectrum figures were plotted using Welch's power spectral density method and a Hamming window (see Matlab^{TM}help file). Four angular frequencies are investigated (Figs. 4.9 and 4.10). In Fig. 4.9 one can clearly see the period doubling from $\omega = 15\frac{\text{rad}}{\text{sec}}$ to $\omega = 30\frac{\text{rad}}{\text{sec}}$ in that a half a frequency was added. In Fig. 4.10, we can see two interesting phenomena. In the top half of the figure, corresponding to $\omega = 53.5\frac{\text{rad}}{\text{sec}}$, we can see that there is a curve on the Poincaré surface, corresponding to quasiperiodic motion. In the bottom half of the figure, corresponding to $\omega = 56.4\frac{\text{rad}}{\text{sec}}$, we can see that there are two regions of five point corresponding to period-10 cycle which continues up to higher frequencies.

4.3.1.3 Lyapunov exponents

As mentioned in Chapter 3, a useful tool for analyzing nonlinear systems, specifically bifurcations and chaotic regions, is the Lyapunov exponents. Lyapunov exponents give the average sensitivity of initial conditions along an orbit. Based on the Poincaré mapping, the region around $\omega = 53.5\frac{\text{rad}}{\text{sec}}$, is identified as potentially being a quasiperiodic and not chaotic. To verify this, we plot the largest Lyapunov exponent and examine whether there is a high sensitivity to initial condition in this region, corresponding to chaos. A plot of the largest Lyapunov exponent of the same parameters as depicted in Fig. 4.8 is shown in Fig. 4.11. We can then assume that this suspicious region is not chaotic but quasiperiodic as was assumed by looking at the Poincaré surface.

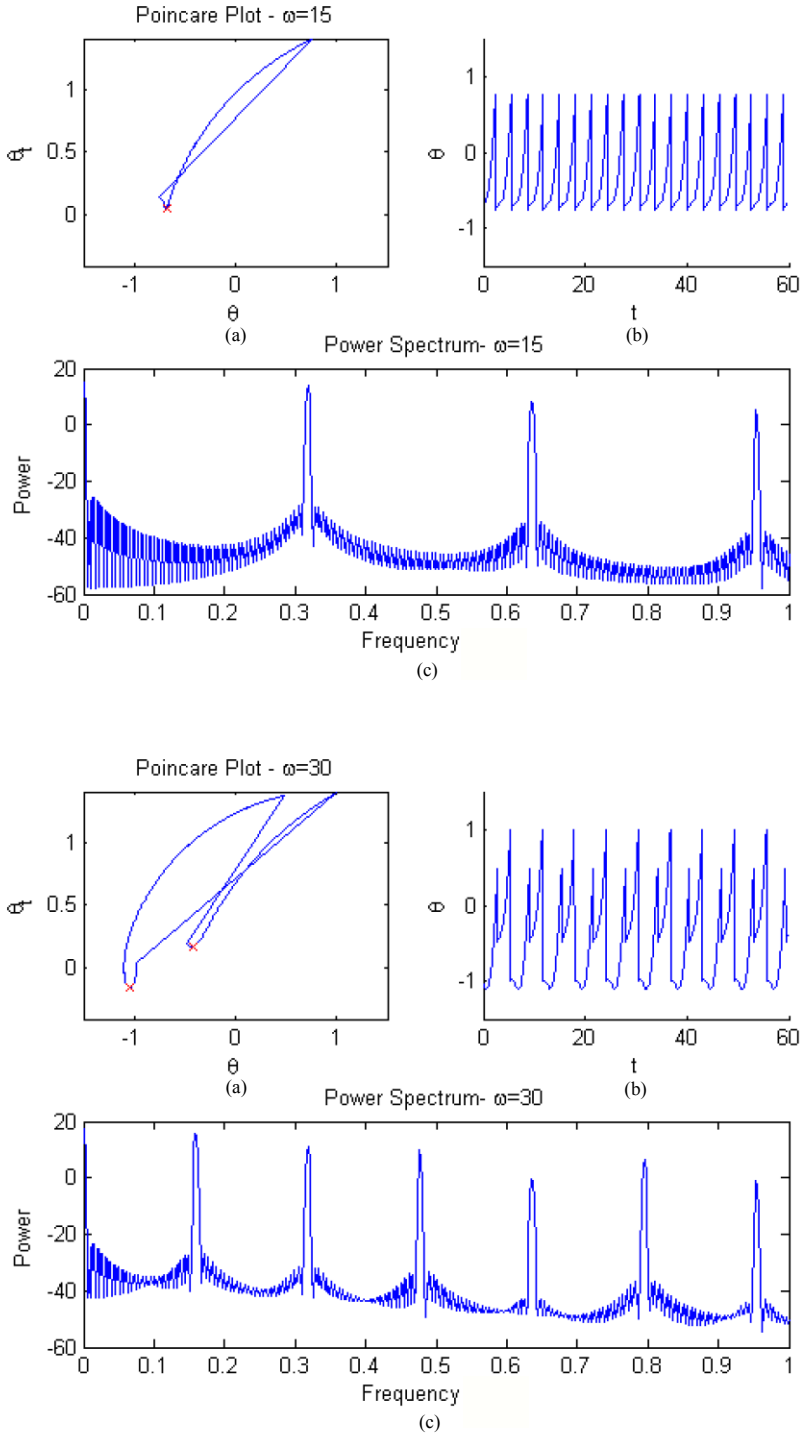

Figure 4.9: Top: $\omega = 15\frac{\text{rad}}{\text{sec}}$, bottom: $\omega = 30\frac{\text{rad}}{\text{sec}}$ a) phase plot (Poincaré points marked with x), b) time series, c) power spectrum. The top Poincaré plot consists of a single Poincaré point, while the bottom Poincaré plot consists of two points together with an additional (nondimensional) frequency in the power spectrum which is half of the fundamental one, revealing a period doubling bifurcation.

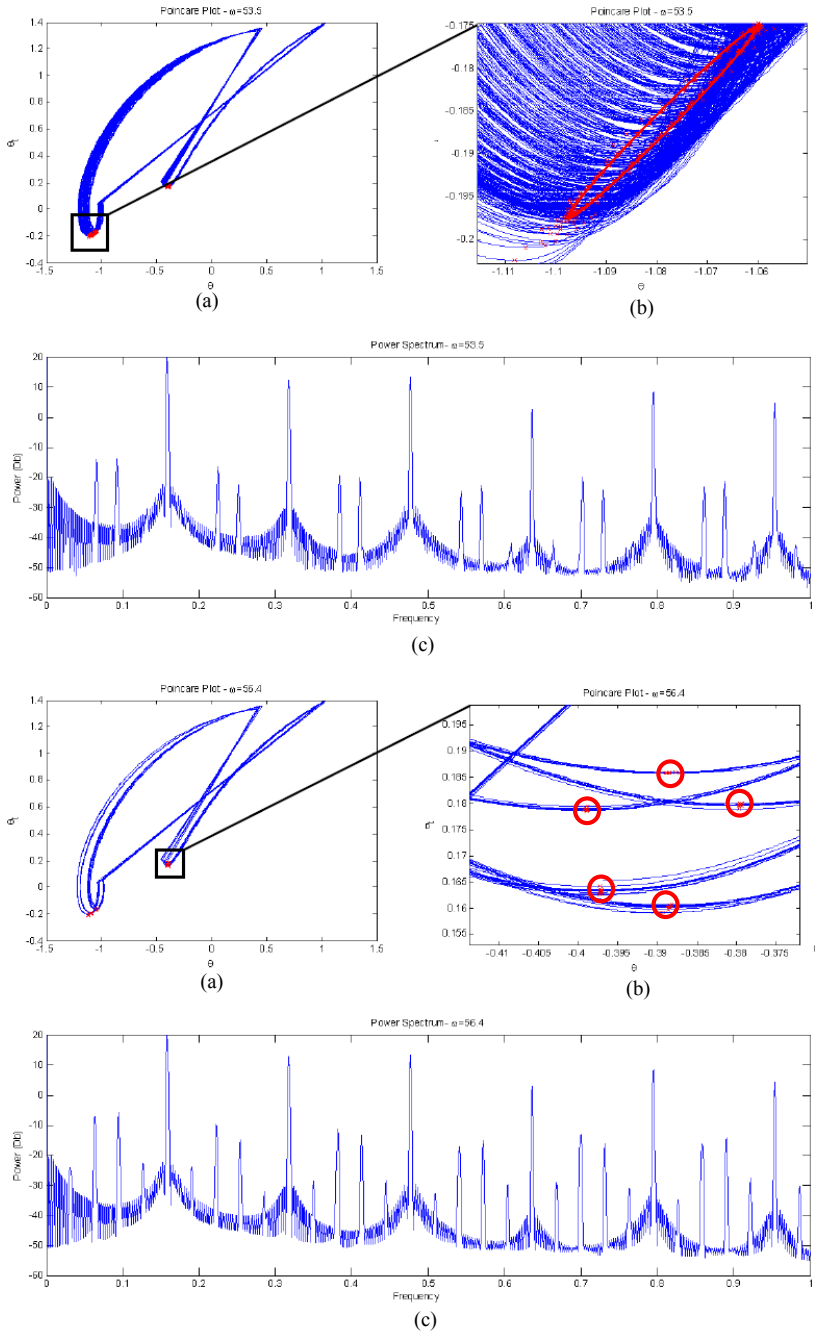

Figure 4.10: Top: $\omega = 53.5\frac{\text{rad}}{\text{sec}}$, bottom: $\omega = 56.4\frac{\text{rad}}{\text{sec}}$ a) phase plot (Poincaré points marked with x), b) close up of Poincaré section with red circles marking the points, c) power spectrum. The top Poincaré plot consists of a closed curve revealing a quasiperiodic solution. The bottom Poincaré plot consists of two sets of five points revealing a period-10 cycle. The power spectrum confirms this hypothesis.

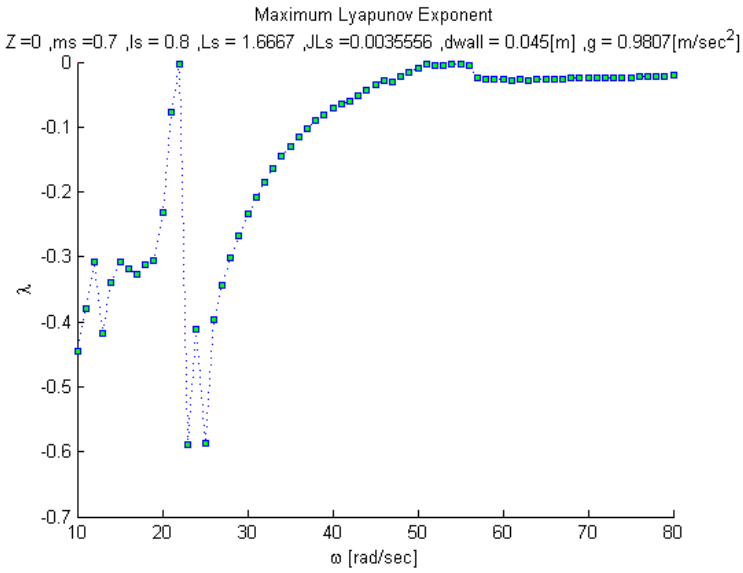

Figure 4.11: Lyapunov exponents plot.

4.3.1.4 Climbing rates

A practical measure of the ability to climb is to measure how far a mechanism climbs during each leap. This corresponds to one Poincaré map. However since asymmetric climbing occurs after the bifurcation points, a better measure might be the average climbing rate, i.e., $\Delta y = \sum_{k=1}^{N} \frac{\Delta y_k}{N}$, where N is the number of maps (approximately 50) and Δy_k is the vertical distance of leap k. Figure 4.12 shows this average leap for the same parameters as the previous results ($A = 0.8$). A noticeable jump occurs at the bifurcation from period-1 to period-2. Apparently, after the period-2 bifurcation, the map initiating at large θ angle climbs significantly more than the period-1 map. Note that period-2 means a leap from one wall with a small θ angle followed by a leap with a large θ angle.

4.3.2 Local stability - varying mechanism parameters

So far the control inputs (A and ω) have been varied and the stability has been investigated. An important extension to this stability analysis is to examine how the stability changes when mechanism parameters are varied. This section examines how varying the link length ratio changes

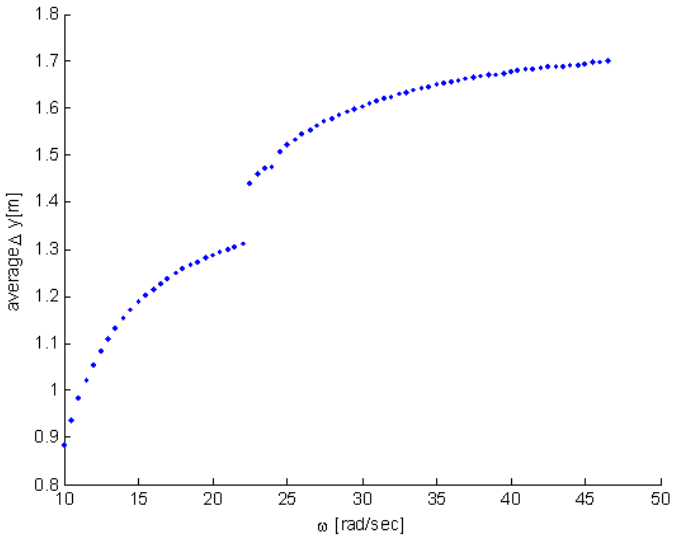

Figure 4.12: Averaged climbing rate.

the local stability.

4.3.2.1 Changing l_s - link ratio

Figure 4.13 shows the bifurcation diagram when l_s is varied. This nondimensional parameter, as described in Appendix B, is the link length ratio $l^* = \frac{l}{L}$, corresponding to the ratio between the body length and the leg length. When the link lengths are almost identical ($l_s \approx 1$) corresponding to the right side of Fig. 4.13, there is a stable period-1 motion. However, when the leg length (L) is elongated, bifurcations start to appear. This is a classic period doubling bifurcation which occurs when one of the eigenvalues exists the unit circle at -1. One can verify the doubling bifurcations by looking at the power spectral density (PSD) and the points on the Poincaré section as shown in Figure 4.14. This plot depicts the PSD (4.14(a)) and points on the Poincaré section (4.14(b)) for different l_s (with largest on top). This Poincaré section plots shows the phase plot and crosses marking the point on the section (Poincaré point). For the period-1 motion (top of plot) only the fundamental frequency (and its harmonics) appears on the PSD. Note that the fundamental frequency it normalized to $\pi/10$. On the corresponding Poincaré section only one point appears. On the second plot, an additional frequency appears. This frequency which is

half of the fundamental one, corresponds to the first period doubling bifurcation. Once again, on the Poincaré section, two points appear. The bifurcations continue with period-4, period-8 on the next plots. The two bottom plots begin showing evidence of the chaotic region. As shown in section 4.3.1, I use the Lyapunov exponents to check if any region potentially has large sensitivity to initial conditions. Figure 4.15 shows the maximum Lyapunov exponent while varying l_s. One can clearly see that bifurcations occur when the Lyapunov exponent grazes zero, but more importunately, the region $0.67 < l_s < 0.71$ is indeed sensitive to initial conditions (positive Lyapunov exp.). This is a strong numerical evidence of chaos at this region.

4.3.2.2 Summary of analysis results

I have shown two proof-of-concept examples of interesting phenomena that occur when varying the control inputs (A and ω) and link length ratio (l_s). This is by no means a comprehensive analysis. The proposed thesis will continue to analyze similar variants and search the space of

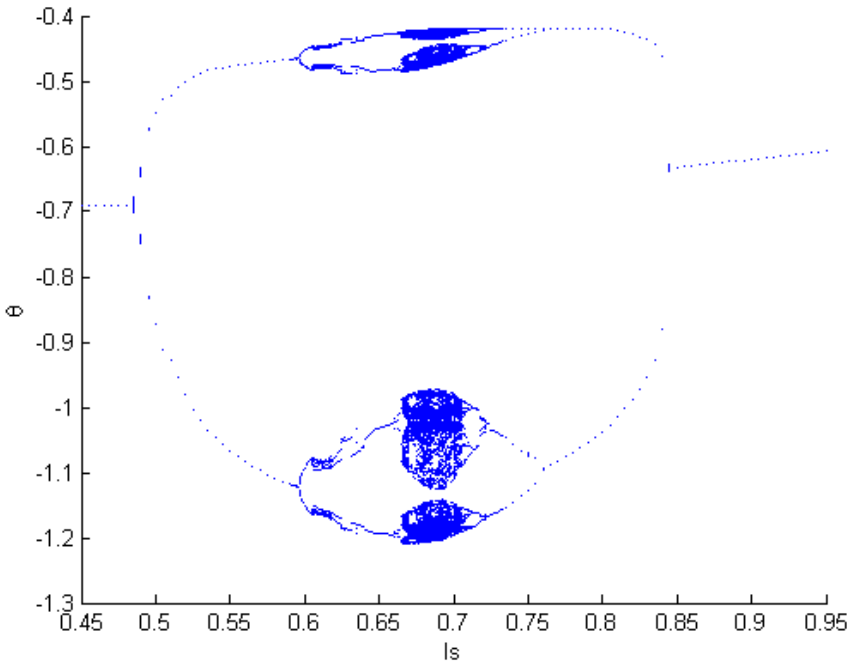

Figure 4.13: Bifurcation plot - varying l_s.

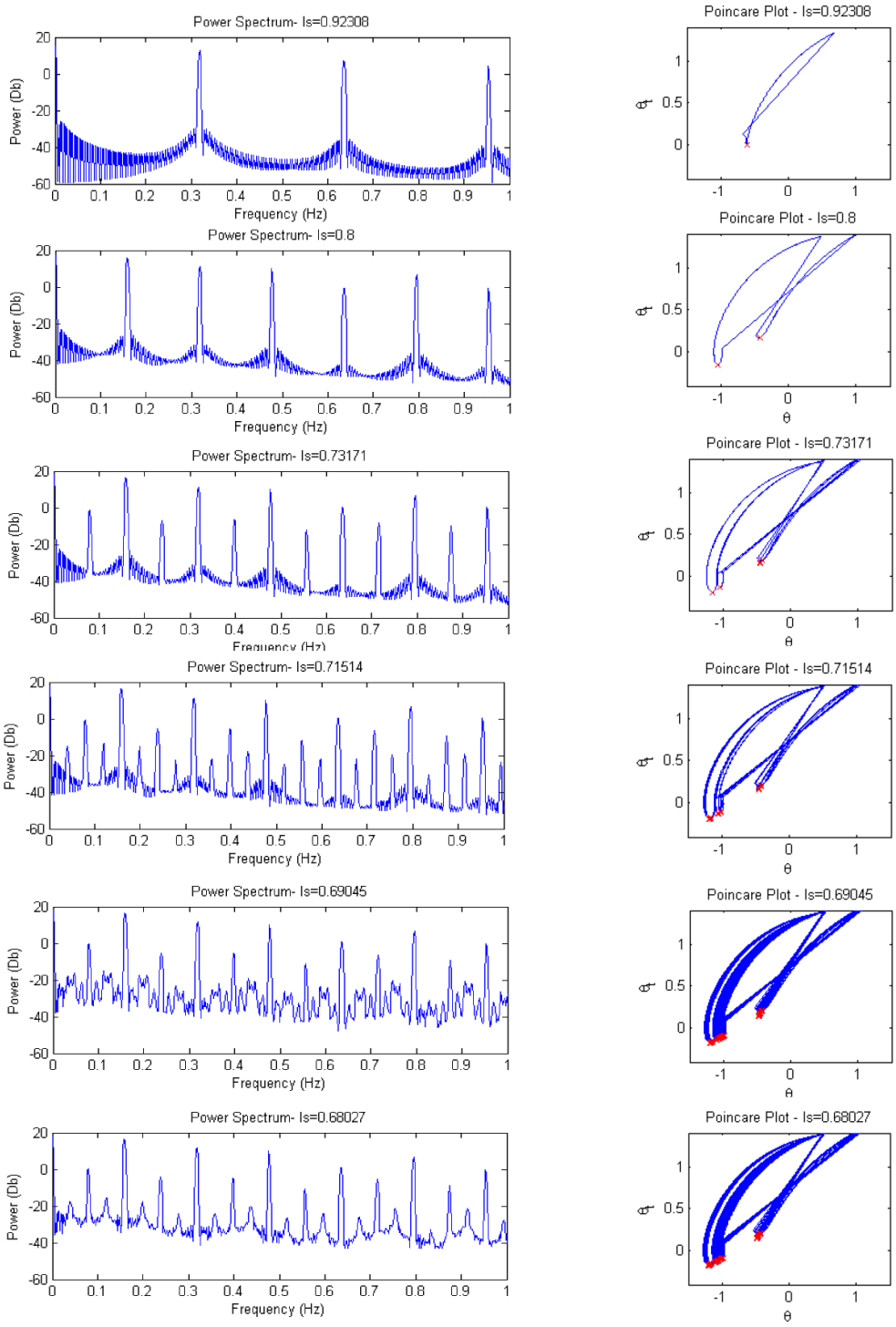

(a) Power spectrum (b) Poincaré sections

Figure 4.14: PSD and Poincaré plots revealing bifurcations with leg length ratio change - l_s from top to bottom: l_s=0.923, l_s=0.8, l_s=0.732, l_s=0.715, l_s=0.69, l_s=0.68. The PSD and the Poincaré plots reveal period doubling bifurcation.

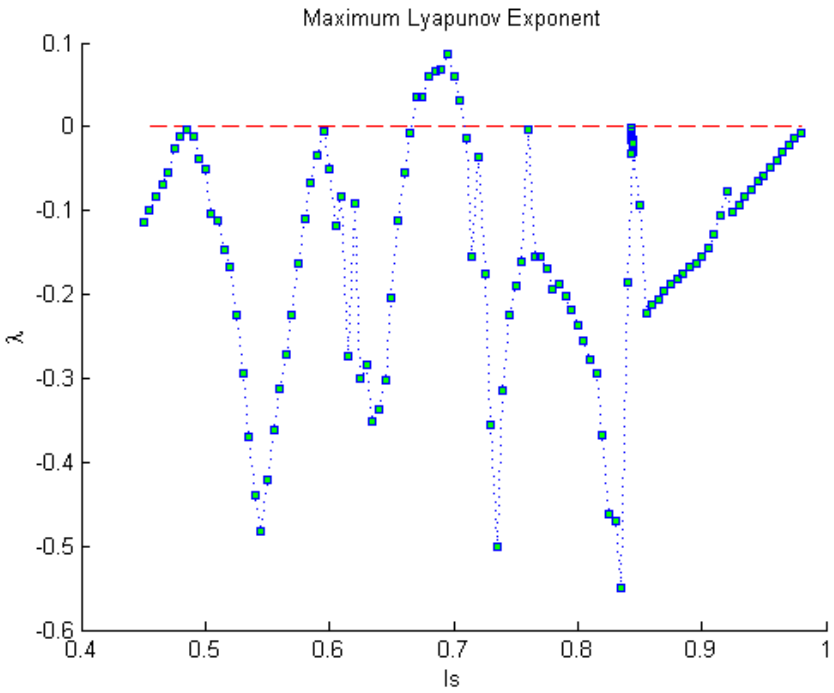

Figure 4.15: Maximum Lyapunov exponent. The central where the Lyapunov exponents are positive infers sensitivity to initial conditions.

mechanism parameters, environment, and control inputs to better understand the parameters.

4.4 Initial experiments

4.4.1 Experimental setup

The experimental setup consists of an air table which reduces the out-of-plane motions. The air table also allows one to lower the effective gravity by inclining the table. As discussed earlier, I am using a tenth of the normal gravitational acceleration. In order to record videos of the experiments and track the mechanism, the Optitrack optical tracking system by NaturalPoint™ (2009) is used. This system tracks passive IR markers at rates of 100[Hz]. Since only 2-D motions are needed to be tracked, we can use a single camera mounted normal to the surface of the air-table (see Fig. 4.16).

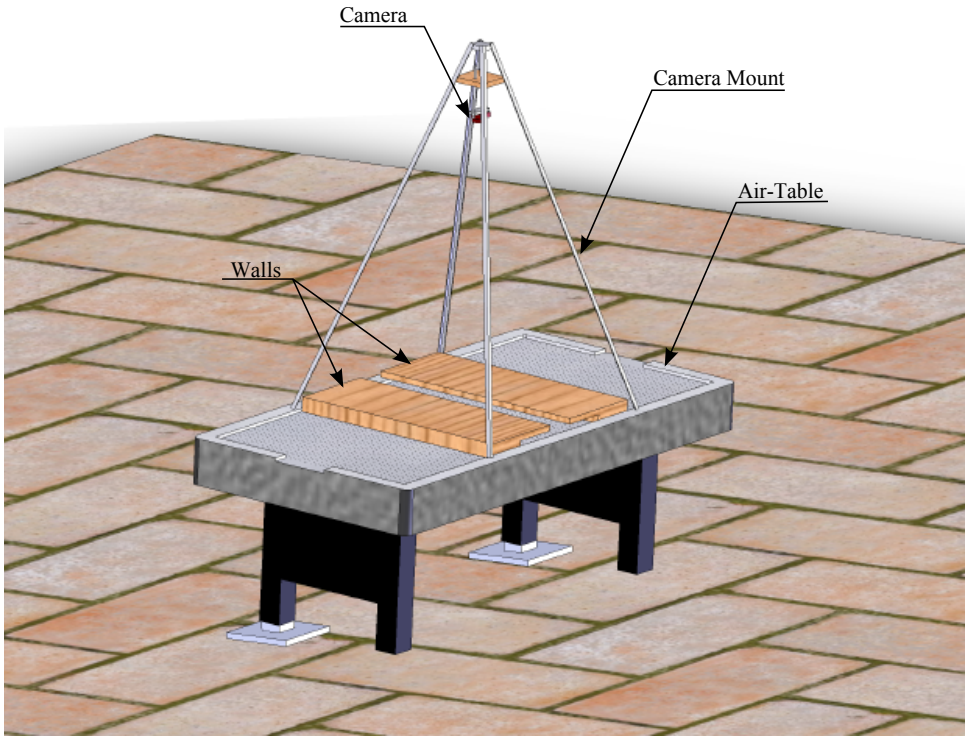

Figure 4.16: Air-table and tracking system mounted above.

4.4.2 Current mechanism design

Our current design (See Fig. 4.17) consists of a disk which increases the surface area between the mechanism and the air-table. On top of the disk the body mass is connected. On this same disk, a servo motor is connected to a light weight leg. The motor produces the sinusoidal motion of the leg. Two ways can be used to achieve this sinusoidal trajectory. Using off board power and controlling it using a pc, or by using an on-board power with an Arduino microcontroller. See Table 4.2 for current mechanism parameters for two experiments with different frequency inputs.

4.4.3 Initial proof-of-concept experiments

Figures 4.18 and 4.20 show a sequence of images of the current design, the first for $\omega = 15.3\frac{\text{rad}}{\text{sec}}$ and the second for $\omega = 19\frac{\text{rad}}{\text{sec}}$. Since it is hard to distinguish between different periods by looking at these images, the corresponding configuration variable plots are given in Figures 4.19

Table 4.2: Nondimensional parameters of current mechanism

Parameter	Description	Value
Mechanism Parameters		
M	Motor mass	0.06 Kg
m	Body mass	0.21 Kg
L	Leg length	0.121m
l	Body length	0.115m
J_L	Leg moment of inertia	9×10^{-5}
d_{wall}	Half of wall gap	0.0635m
g	Gravity	$0.9807 \frac{\text{m}}{\text{sec}^2}$
A	Amplitude	0.3
ω	frequency	$15.3 \frac{\text{rad}}{\text{sec}}$ and $19 \frac{\text{rad}}{\text{sec}}$
Non Dimensional Parameters		
m^*	Mass ratio $\frac{m}{m+M}$	0.7778
l^*	Link length ratio $\frac{l}{L}$	0.9504
L^*	Link to walls gap ratio $\frac{L}{d_{wall}}$	1.9055
J_L^*	Nondimensional inertia $\frac{J_L}{L^2(m+M)}$	0.0228
γ	Nondimensional gravity $\frac{g}{d_{wall}\omega^2}$	0.0660 and 0.0428
A	Amplitude	0.3

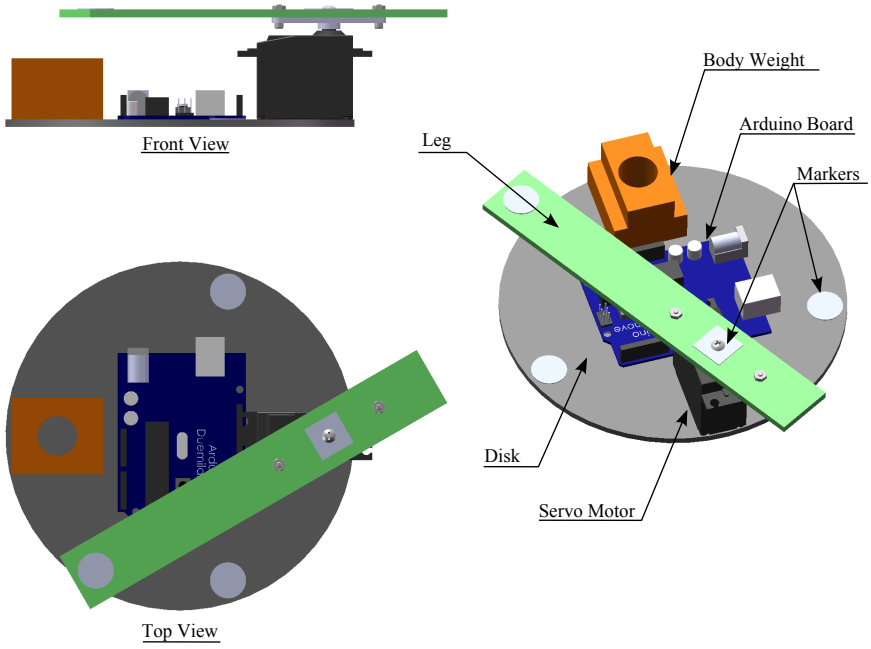

Figure 4.17: Current mechanism design.

and 4.21. These plots are obtained by tracking the four markers using the Optitrack system. As was assumed, ϕ is approximately sinusoidal, other than small perturbations during impact. Observing the θ one can see that for the relatively low frequency a symmetric, period-1 exists. For the higher frequency a period-2 appears. On these θ plots, the crosses mark the points on the Poincaré surface including the flip after each impact.

4.5 Summary of initial work

This chapter captures the essence of the open-loop analysis of this minimalist, underactuated robot. The chapter began by introducing the mechanism's model and showing how the three phases can be simulated. It continued by showing typical nonlinear analysis that reveled bifurcations both when the control inputs were varied and also when the link length ratio was varied. The next, proposed work chapter will enumerate what will be added to this open-loop analysis and what other extensions are proposed.

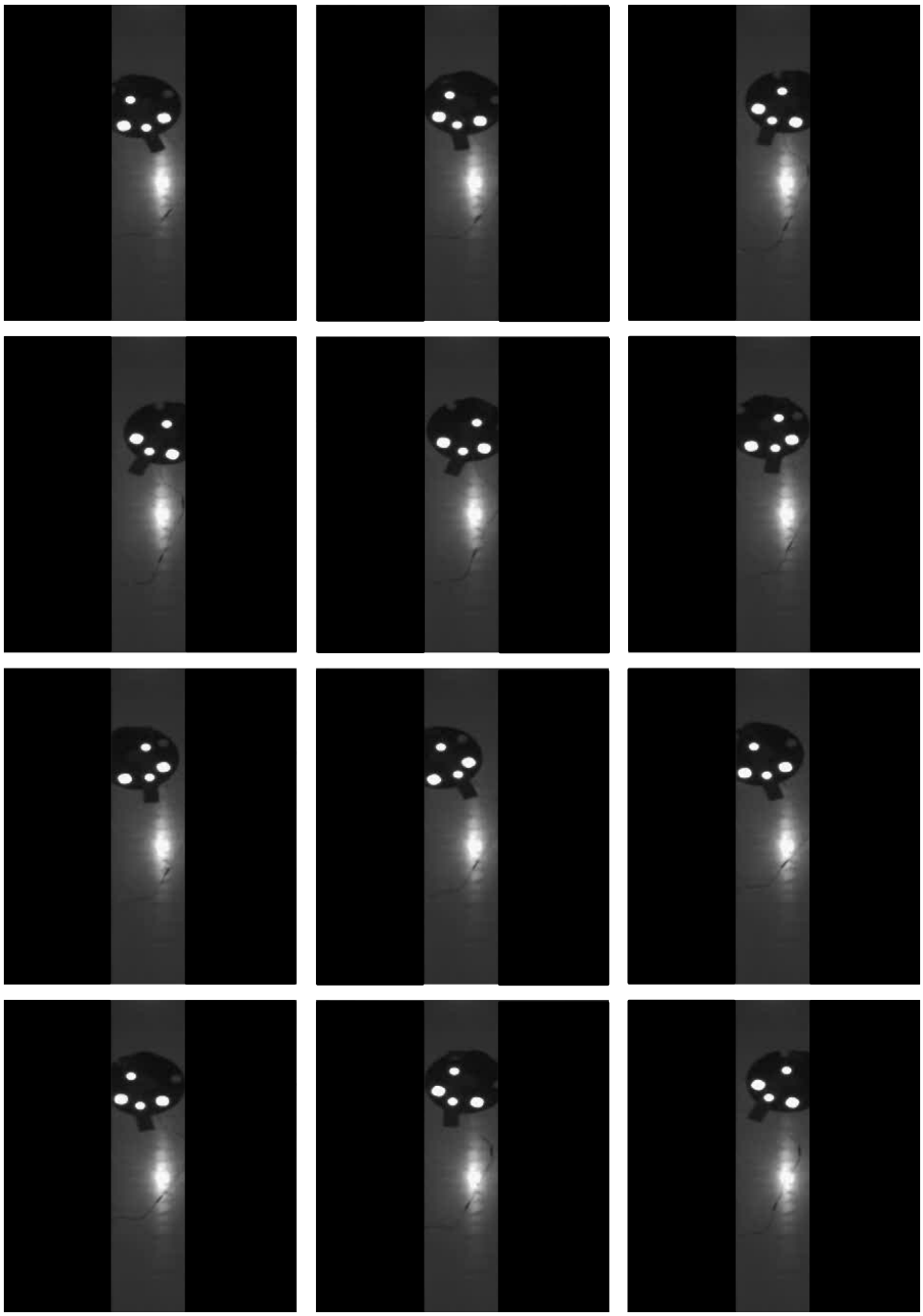

Figure 4.18: Proof-of-concept experiment - $\omega = 15.3\frac{\text{rad}}{\text{sec}}$ – image sequence 1/30 sec apart.

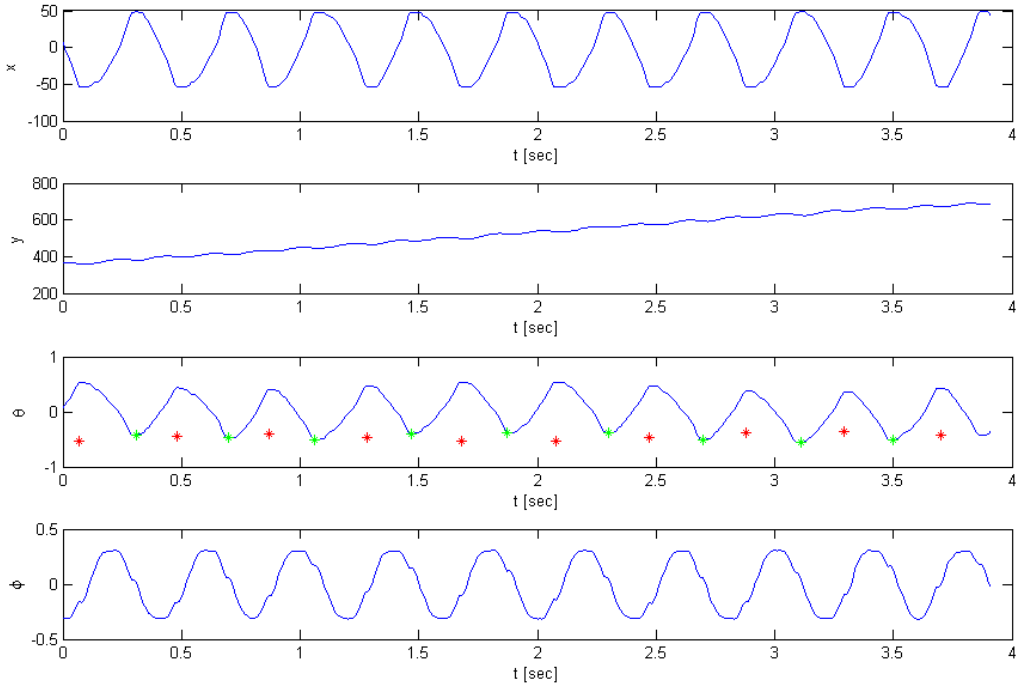

Figure 4.19: Proof-of-concept experiment - $\omega = 15.3\frac{\text{rad}}{\text{sec}}$ – plot of configuration variables. Crosses mark the points on the Poincaré section, including the flip. The plot of the leg angle θ reveals a symmetric period-1 climbing pattern. The plot of the angle ϕ, between to the two links follows the desired sinusoid.

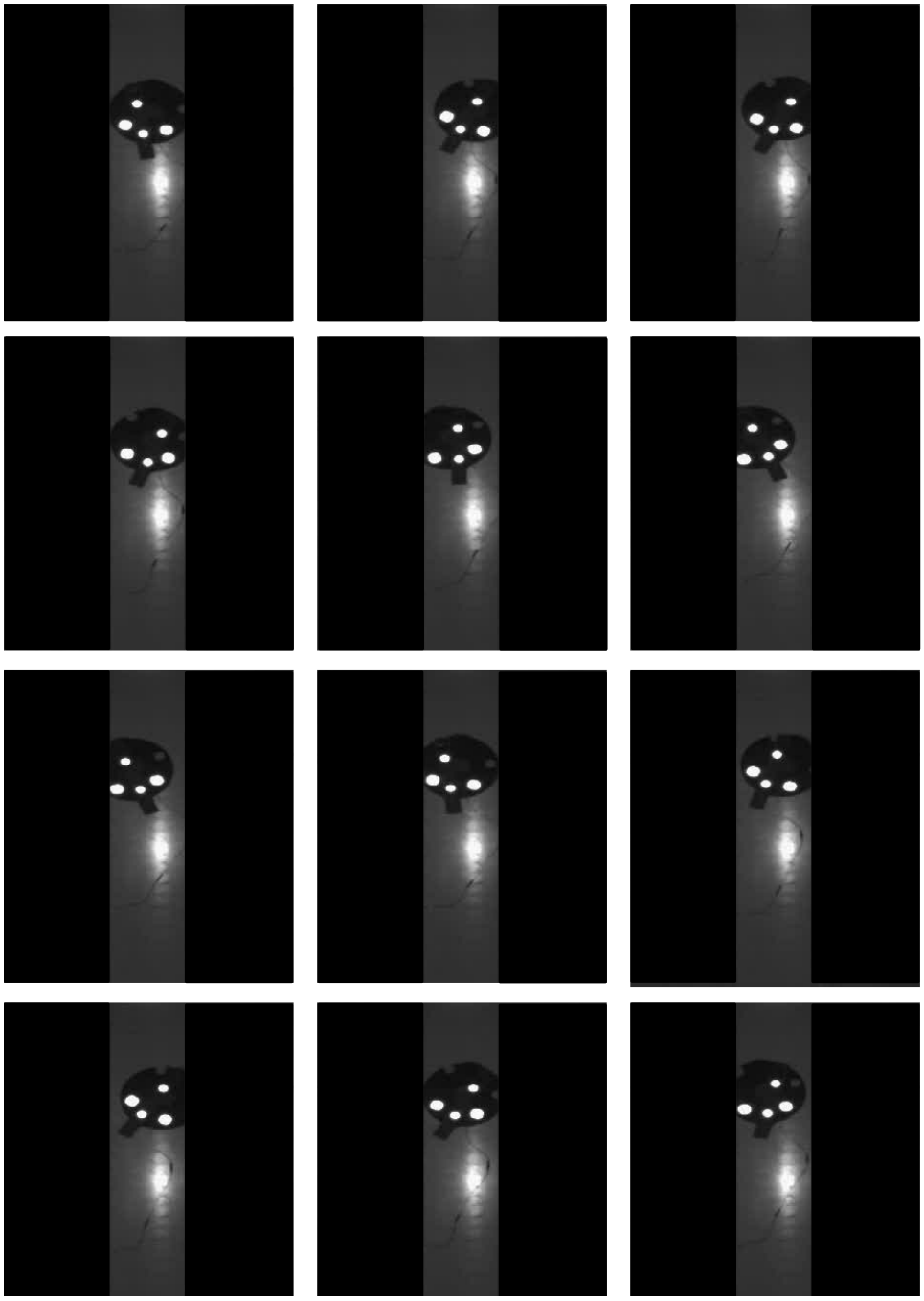

Figure 4.20: Proof-of-concept experiment - $\omega = 19\frac{\text{rad}}{\text{sec}}$ – image sequence 1/30 sec apart.

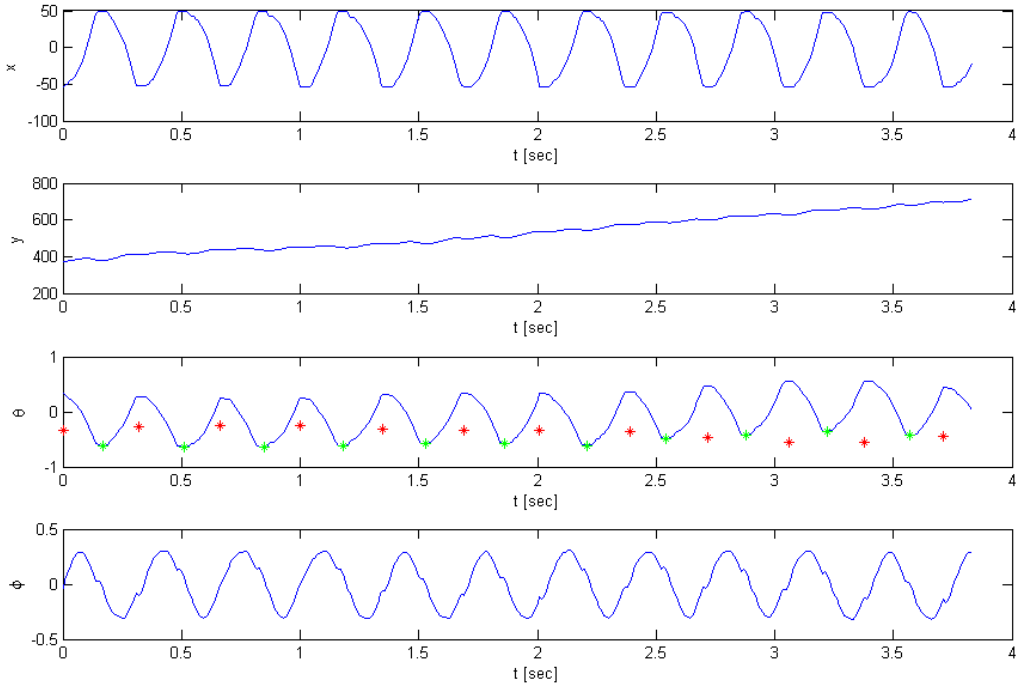

Figure 4.21: Proof-of-concept experiment - $\omega = 19\frac{\text{rad}}{\text{sec}}$ – plot of configuration variables. Crosses mark the points on the Poincaré section, including the flip. The plot of the leg angle θ reveals a non-symmetric period-2 climbing pattern. The plot of the angle ϕ, between to the two links follows the desired sinusoid.

Chapter 5

Proposed Work

The proposed thesis work first addresses the improvements and extensions of the current analysis of the open-loop stability. This includes generalizing the equations of motion and searching the parameter space for stability changes. Furthermore, I intend to optimize the mechanism for local stability and extend the stability analysis from local stability into global stability (basin-of-attraction). Once open-loop climbing is optimized, I will attempt to achieve climbing in a more complex environment by adding a simple control loop. Specifically, I will replace the two parallel walls with piecewise linear walls and to achieve stable climbing in this environment, a simple control loop will be incorporated, which only needs to know the location of the mechanism in the a priori known environment.

5.1 Open-loop stability and implications

5.1.1 Improvements and extensions

1. As discussed in Sec. 4.2.3, the Poincaré section is simplified by assuming that the transition to flight phase occurs when $\phi = 0$. In reality this assumption is not correct for all the variations of the mechanism. I propose to add the correct transition state which occurs

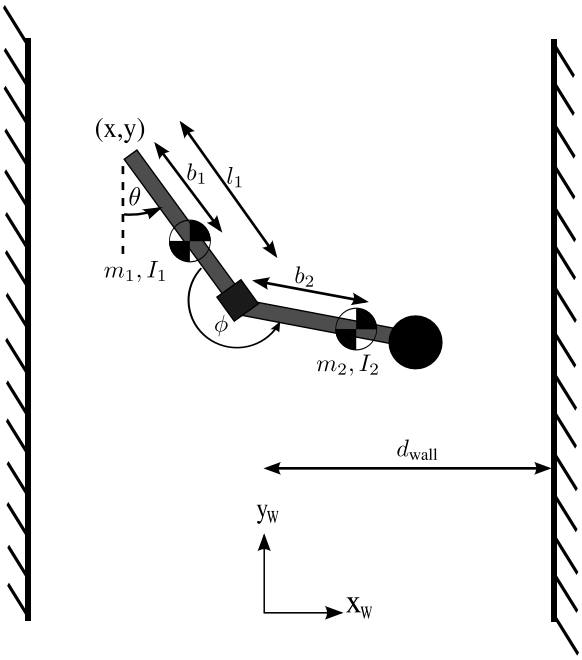

Figure 5.1: Schematics of new two link mechanism climbing between two parallel walls with added parameters.

when the contact forces of the link with the wall changes sign using Eq. 3.6.

2. The equations of motion which were used in Chapter 4 do not apply to a general two link robot. A more general model can be obtained if more parameters are added (as in Fig. 5.1). This model adds two additional parameters; inertia to the main body (I_2) and enabling the COM of the leg be in an arbitrary position (b_1), unlike the lumped mass at motor as was previously proposed.

3. The modeling in Chapter 4 assumes that only the distal end of the leg collides with the walls. This of course will not hold true for any arbitrary mechanism or control inputs. By using LCP formulation – linear complimentary problem as described in (Stewart and Trinkle, 1996), it is relatively easy to generalize the possible colliding points with the wall and allow stick slip transitions.

5.1.2 Parameter search

So far in Chapter 4 I have showed results for a few, well picked mechanisms and control inputs. Performing a wider search over the parameter space, including environment, mechanism, and control parameters, will enable us to better understand the system. Knowing which parameters change the periodicity of the system, which ones increase (or decrease) the basin-of-attraction of the system can give valuable information on the mechanism.

5.1.3 Global stability – basin-of-attraction

Chapter 4 discusses the stability analysis of the climbing mechanism. Specifically, the local orbital stability was investigated by first finding the fixed point, then linearizing around this point and lastly looking for the eigenvalues which correspond to the rate of convergence (or divergence) from the limit cycle. This stability criterion is only applicable locally around the fixed point. Global stability would entail finding the basin-of-attraction of the attractors. That is, what set of initial conditions will converge to one of the fixed points.

This investigation can be done by discretizing the state space and forward simulating these initial conditions until they converge on an attractor. This method is time and computation consuming. Alternatively, a different technique called cell mapping can give a relatively good estimate of regions of attractions in the state space. In the cell mapping technique, described in full in (Hsu, 1997), the phase space is first discretized into a large number of small cells. One Poincaré map is numerically calculated once for the center of these cells and the information is recorded. Cells mapped outside of the discretized area are marked as mapped to a "sink cell". Sink cells are also mapped back to themselves. All the dynamic information, up to the precision of the grid division, is now contained in these simple pointers. It is now possible to iterate these pointers to find periodic cycles.

Instead of calculating the complicated Poincaré map from each initial condition until convergence, which can be about 10,000 cycles, this method only computes the Poincaré map once for

each cell. The main disadvantage is that depending on the resolution of the discretization, this method can falsely classify wrong periodicity, though, it usually provides a good idea of where the relevant regions of attractions are.

I propose to use this method in order to find the global stability of the system. This will provide information of which states will converge into period-1 cycles, period-2 or to an unstable cycle (sink cell).

5.1.4 Optimal open-loop control

What is the fastest possible climbing rate of the climber? What is the most stable climber? What is the least amount of control input needed for a climber to climb? These questions might all be important when analyzing a climbing mechanism. Part of the problem is that optimizing one objective usually hurts the other. For instance, the most stable mechanism might be very slow. One way to find a good climbing mechanism is to try to optimize these functions. Mombaur et al. (2005b) showed how an optimization scheme can be performed on a one- or two-legged robot. By employing a double loop optimization, i.e., optimizing stability while in the inner loop optimizing control inputs, the authors were able to find an optimal control, stable, open-loop hopping robot. In a similar way, I propose to optimize climbing rates together with the smallest control inputs. In our case this will correspond to minimal amplitude and frequency of the sinusoid movement while keeping the mechanism stable.

5.2 Uneven terrain – toward piecewise linear walls

One natural evolution in complexity for this research is to climb on a harder terrain. One possible extension is to move from the parallel walls assumption to piecewise linear walls. If the robustness of the system is extremely high, i.e., large basin-of-attraction, the mechanism might even climb this complex terrain stably without intervention. The more interesting question, however,

will arise when the width change exceeds what the stable climber can handle. The a priori knowledge of the stable regions , such as the local stability plot in Fig. 4.7, can give rise to a transition formulation from one wall gap to the next. For instance, if we care to only climb in a period-1 gait, we can find the transition from one period-1 region for the first gap and change the control inputs such that in the second gap we will stay in the period-1 gait. There are two caveats in this approach. The first is that there must be a sudden change in the control inputs at the correct time. More crucially, the a priori knowledge from the open-loop study is only correct for steady state dynamics, but in this scenario there is a constant change in the environment parameter. The next subsection (5.2.1) will try to address these problems.

5.2.1 Control and planning

As mentioned previously we are interested in transitioning from one wall gap to another without losing stability. I will assume that the terrain is known a priori and for simplicity we aim to climb only in a symmetric period-1 gait. This assumption can later be extended to other period-k gaits. For a given set of mechanism parameters and environment such as different wall gaps, the period-1 regions in the $A-\omega$ plane will be searched. This stability analysis will then be repeated for different wall gaps. As a simplified illustration of this form of analysis refer to Fig. 5.2. Note that in Fig. 5.2 the basin-of-attraction might not be realistic, but it gives a nice illustration of the problem. In Fig. 5.2(b) the overlapping stable, period-1 regions for the different wall widths are identified, allowing one to construct the feasible transition from one wall width to another. The problem has now been converted into a simple graph (Fig. 5.2(c)), which is more easily searched to find a feasible transition plan. As an example, if we start in a stable climbing in wall gap(1) and are interested in transitioning to gap(3) we must first change A and ω in order to transition safely to gap(2). After passing gap(2) we then change A and ω once again to reach gap(3). We must still take care of the problem, mentioned earlier, of using steady state analysis in a situation where we clearly have transient movements. For this, we must also include the global stability

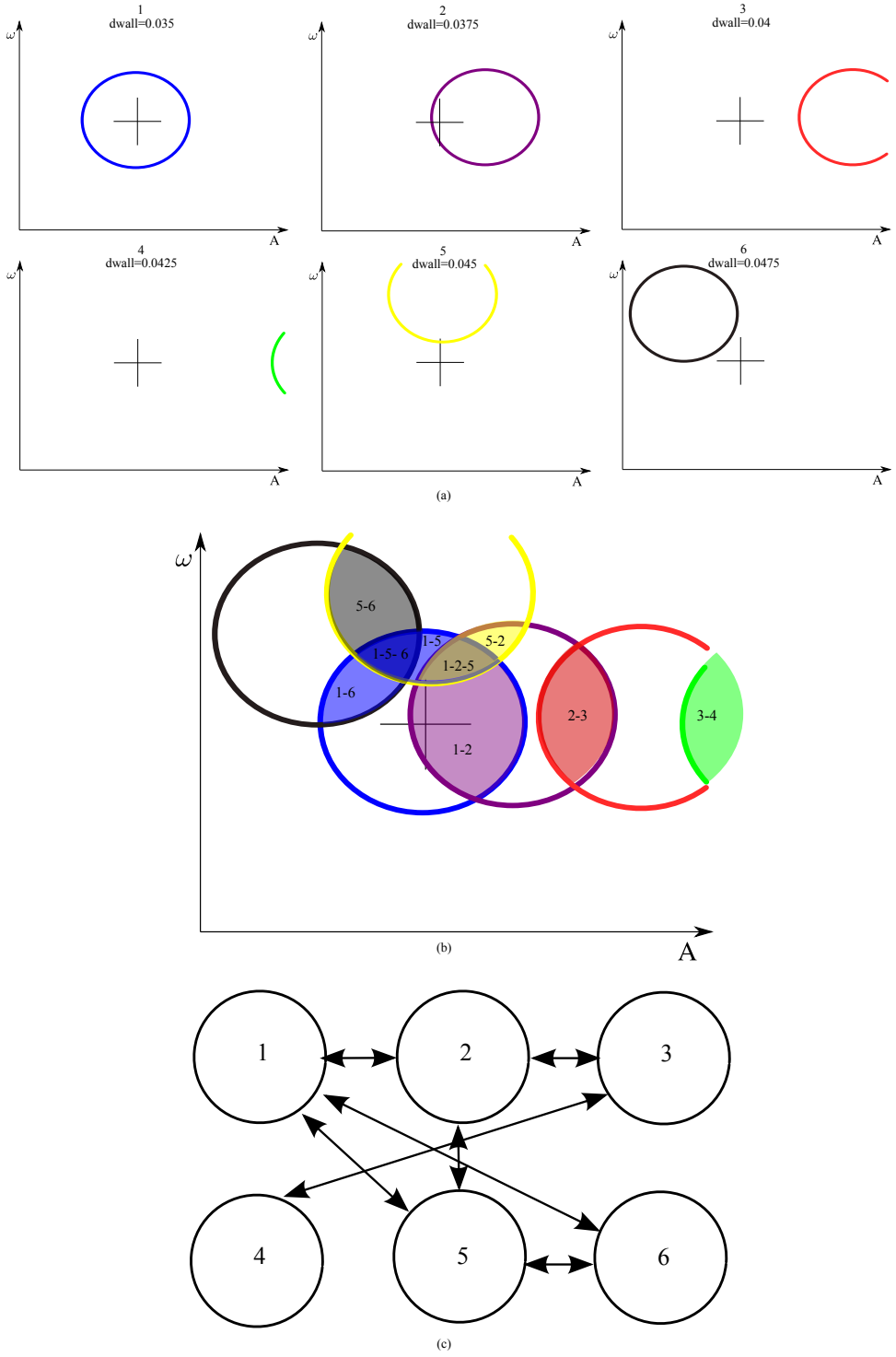

Figure 5.2: (a) A simplified example of six basin-of-attraction for six different wall gaps - ellipses represent the basin of an attractor, (b) The intersections of the basin-of-attractions are labeled. These intersection correlate to possible transitions from one wall gap to another (c) Representation of the transition graph. Edges mark valid transitions from one attractor to the basin of another.

analysis (basin-of-attraction) we have found earlier. This will increase the space. For example, the 2-D A-ω plot of Fig. 5.2 might be a 4-D ($A - \omega - \theta - \dot{\theta}$) plot also containing the basin-of-attraction information. It will then be possible to safely transition from gap(1) to gap(2) while staying in the basin-of-attraction of gap(2).

5.2.2 Proposed design

As mentioned earlier, one of the design concerns is out-of-plane bounces during impact. The first design improvement will be to construct a balanced mechanism to reduce these bounces. Moreover, I have shown that the link length ratio is an important parameter which changes the behavior of the mechanism dramatically. I propose to add a functionality in the design to allow control over this link length ratio. This ratio will be controlled by adding a negligible mass foot to the end of the leg as shown in Fig. 5.3. The T-shaped foot will be placed on a linear slide and will be actuated using stepper motor. The T-shape foot not only enables a change in the link ratio, but can also be used to relax the assumption of the body mass moving over the walls, since it increases the width of the leg. This link ratio change will now be used to first correlate the bifurcations with change of l_s and later may also be used move from one attractor to another depending on the environment.

5.3 Power efficiency, and more efficient prototypes

If time permits I will try to explore more efficient climbing mechanism. One such mechanism which we are currently building uses two fiberglass springs as legs (bowlegs). These springs are extremely efficient with approximately 80%-90% efficiency. Although this climbing mechanism might be very efficient, it does not have the same open-loop stability aspect as the proposed DSAC mechanism. To make the proposed mechanism more efficient we may add a telescoping leg in the foot that collides with the wall. Alternatively, we may control the transition from

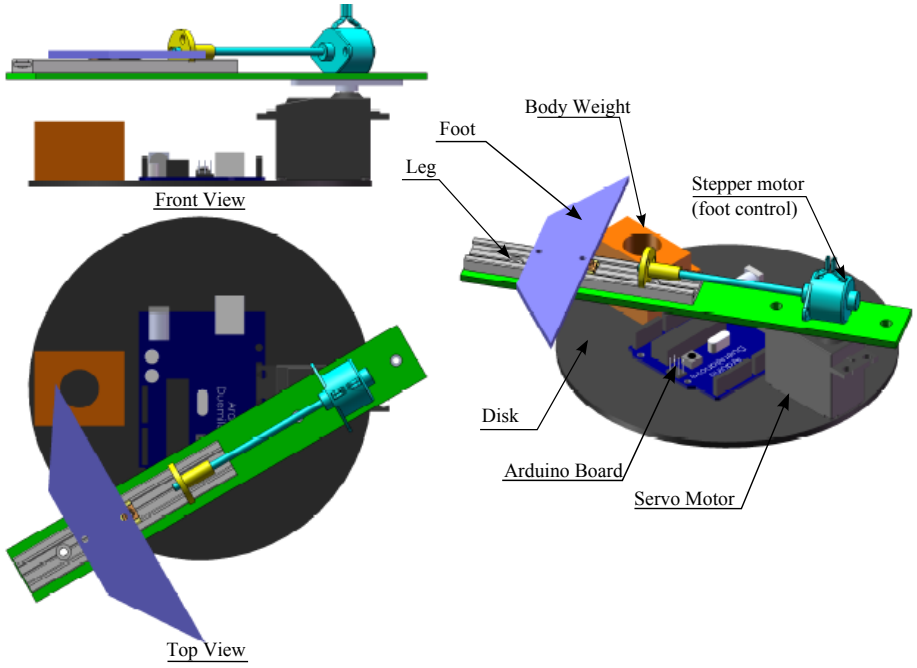

Figure 5.3: Sketch of proposed mechanism design with varying length foot.

flight to impact phase by velocity matching. This might enable a smooth transition from flight to stance without the need of an instantaneous loss of energy during the plastic collision. I will also explore a theoretical bound of zero energy cost in climbing. Gomes and Ruina (2005) show that a zero energy walking gait is possible, albeit not stable. Is such zero energy cost possible in climbing?

5.4 Experimental validation

The experimental validation is an important part of the thesis work. I propose to build an accurate, modular, and tetherless prototype that will validate the theoretical findings. The main problem of this current mechanism design is out of plane bounces. Since the mechanism is not balanced around the impact plane it bounces during impact. I will deal with this problem by trying to design a more symmetric mechanism which will be balanced, i.e., center of mass on the impact plane while trying to reduce non-diagonal inertia elements. Also, while experimenting I have observed that since the length of the chute is relatively small ($\approx$ 1m) the motions did

not reach a steady state. Moving to the long axis of the air-table doubles the climbing time and enables the transients to disappear. Furthermore, introducing damping into the model and the experimental setup should decrease the time of transients. Moreover, This prototype will also include a motor that controls the leg length in order to verify the bifurcations relative to leg length change. As the final experimental goal, I propose to use feedback from the tracking camera to climb inside piecewise linear walls.

5.5 Timeline

I expect to complete the thesis by the end of the summer semester of 2010. My tentative research plan includes the following components

Summer 2009

- Improvements and extensions of the open-loop climbing analysis.
- Design and build a more accurate model for open loop climbing. This includes the reduction of out-of plane bounce and tetherless control over amplitude and frequency, together with the ability to vary the leg length.

Fall 2009

- Global stability - basin-of-attraction using the cell mapping technique.
- Optimization of stable climbing.
- Run validation experiments for open-loop climbing. This includes experiments of stability regions together with bifurcation relative to parameter change.

Spring 2010

- Planning and control for piecewise linear walls.
- Run validation experiments for piecewise linear walls.
- Begin writing dissertation.

Summer 2010

- Continue writing dissertation.
- Thesis defense.

5.6 Conclusions

The mechanism explored in this thesis aims to perform stable climbing with minimal design and control complexities. Unique to this mechanism is that it uses dynamic motions to achieve this goal. As it stands, it can achieve a simple climbing task comparable to what quasi-static robots can accomplish, with only a single motor and without any complex controls.

The dynamic motions uniquely used by this mechanism entail the potential not only to climb with a low number of actuators, but also to accomplish more complex tasks, such as overcoming obstacles, and to climb quickly and efficiently. Even in open loop, the DSAC proposed here, in fact surpasses quasistatic climbers in the relatively wide range of wall gaps it can robustly climb.

To deal with more versatile terrain, I am proposing to incrementally add complexity to this minimalist mechanism. In particular, the proposed work includes providing the mechanism with the ability to sense the environment and accordingly change its control inputs. This is not a complicated closed loop. The two links will still be constrained to move in a simple sinusoidal, however the amplitude and frequencies will now be changed as a function of the wall gap.

One might ask why minimalism is even beneficial. Why should we want simple design with only a single motor and no complex control? One big motor may be more complex (or costly) than four small motors. Although true in some respects, minimalism still provides a huge advantage in others. One example is when a mechanism is shrunk to small scales. In such cases, complex elements including springs, bearings, and linear motors are almost impossible to package. However, a mechanism which can achieve the task using a single revolute motor can be relatively easily miniaturized.

To summarize, the proposed DSAC serves as a good example of how dynamic motions can help design a mechanism in a minimalist way which can achieve results comparable to other mechanisms with more complex design and control. So far I have analyzed the open-loop stability characteristic of the mechanism, recognizing how some parameters change the climbing motion and some are crucial to its stability. Adding minimal complexity in control will hopefully enable it to reach greater objectives.

Appendix A

Nondimensionalizing

A.1 Nondimensionalizing differential equations

The use of nondimensionalizing equations of motion is a practical tool in analyzing dynamical systems. This method can reduce the number of parameters and introduce important nondimensional ratios instead of specific parameters.

Nondimensionalisation scales each variable, dependent and independent, by a characteristic value which results in a nondimensional variable.

This methods has several uses:

1. It finds dimensionless groups which are ratios of parameters which are the one who control the differential equation.
2. because the coefficients of the differential equation are now dimensionless it allows to compare terms and find the dominant versus negligible terms.
3. gives intuition of what should be varied in an experimental setup.
4. can reduce the number of parameters by up to the number of fundamental units involved in the equation. In our case of mechanical system, this procedure can reduce by up to three parameters corresponding to the following fundamental units: mass, length, and time.

Follows is the procedure in nondimensionalizing a differential equation.

1. List all variables including dependant and independent variables.
2. For each variable choose a characteristic parameter in order to define a new, nondimensional variable. For example, for a variable x (with units of meters $[\mathrm{m}]$) one might choose a characteristic length of l_o. The new nondimensional variable will now be: $\bar{x} = \frac{x}{l_0}$. Do not forget to also nondimensionalize time. There is no unique way to choose the characteristic parameters. However, different choices will change the ratios.
3. Rewrite the differential equations with the new nondimensional parameters. Note that in order to rewrite the derivatives w.r.t time one must use the chain rule. For example: for an x variable ($[\mathrm{m}]$) and time ($[\mathrm{s}]$), let us choose characteristic length and time such that the new nondimensional variable are: $\bar{x} = \frac{x}{l_0}$ and $\bar{t} = \frac{t}{t_0}$. Now the first time derivative of x w.r.t time is:
$$\frac{dx}{dt} = \frac{d\bar{x}x_0}{d\bar{t}}\frac{d\bar{t}}{dt} = x_0\frac{d\bar{x}}{d\bar{t}}\frac{1}{t_0} = \frac{x_0}{t_0}\frac{d\bar{x}}{d\bar{t}}$$
The derivative is now fully dimensionless and the units are all "outside" of the derivative, $\frac{x_0}{t_0}$ in our example.
4. as stated before, from the previous step all the units are outside of the derivatives, hence if dividing the equations by one of these coefficients will normalize the equations and yield nondimensional coefficients (or parameters).

Appendix B

Equations of Motion

B.1 General equations of motion

This section will derive the general equations of motion of the three phases.

B.1.0.1 Free flight phase

Using the Lagrange method the energy must be first found. For that, the kinematics including the position of the two masses, then velocities are found - see Fig. B.1 for symbols.

$$r_M = \begin{bmatrix} x + L\sin\theta \\ y - L\cos\theta \end{bmatrix} \quad r_m = \begin{bmatrix} x + L\sin\theta - l\sin(\theta+\phi) \\ y - L\sin\theta + l\sin(\theta+\phi) \end{bmatrix} \tag{B.1}$$

where x, y, θ and ϕ are actually time dependant, i.e., $x(t)$, $y(t)$, $\theta(t)$ and $\phi(t)$.

Velocities of masses:

$$v_m = \frac{dr_1}{dt} = \begin{bmatrix} x' + L\cos\theta\,\dot{\theta} \\ y' + L\sin\theta\,\dot{\theta} \end{bmatrix} \quad v_m = \begin{bmatrix} x' + L\cos\theta\,\dot{\theta} - l\cos(\theta-\phi)(\dot{\theta}-\dot{\phi}) \\ y' + L\sin\theta\,\dot{\theta} - l\sin(\theta-\phi)(\dot{\theta}-\dot{\phi}) \end{bmatrix} \tag{B.2}$$

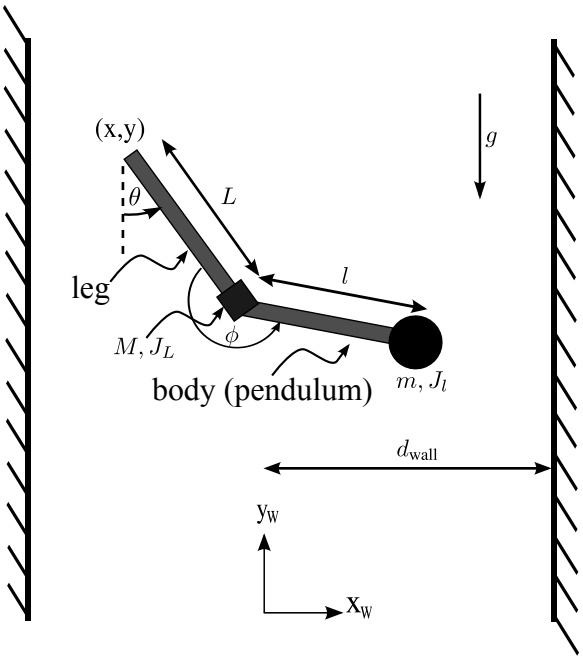

Figure B.1: Schematics of two link mechanism climbing between two parallel walls (same as Fig. 4.1).

The Lagrangian is written as $L = T - V$ where the kinetic and potential energies are:

$$\begin{aligned} T =& \frac{1}{2}Mv_m^2 + \frac{1}{2}mv_m + \frac{1}{2}J_L\dot{\theta}^2 = \\ & \frac{1}{2}\left(J_L\dot{\theta}^2 + M\left((\dot{x} + L\cos\theta\dot{\theta})^2 + (\dot{y} + L\sin\theta\dot{\theta})^2\right)\right) + \\ & \frac{1}{2}\left(m\left(\left(\dot{x} + L\cos\theta\dot{\theta} + l\cos(\theta-\phi)(-\dot{\theta}+\dot{\phi})\right)^2 + \left(\dot{y} + L\sin\theta\dot{\theta} + l\sin(\theta-\phi)(-\dot{\theta}+\dot{\phi})\right)^2\right)\right) \end{aligned} \tag{B.3}$$

$$V = -Mgr_M - mgr_m = g(-L(m+M)\cos\theta + lm\cos(\theta-\phi) + (m+M)y) \tag{B.4}$$

Next,Eq. 3.1 from Sec 3.1 is used to find the equations of motion

$$\frac{d}{dt}\frac{\partial L}{\partial \dot{q}_i} - \frac{\partial L}{\partial q_i} = 0 \tag{B.5}$$

In matrix form

$$M(q)\ddot{q} + h(q,\dot{q}) = 0, \tag{B.6}$$

where

$$M(q) = \tag{B.7}$$

$$\begin{pmatrix} m+M & 0 & L(m+M)\cos\theta - lm\cos(\theta-\phi) \\ 0 & m+M & L(m+M)\sin\theta - lm\sin(\theta-\phi) \\ L(m+M)\cos\theta - lm\cos(\theta-\phi) & L(m+M)\sin\theta - lm\sin(\theta-\phi) & J_L + l^2m + L^2(m+M) - 2lLm\cos(\phi) \end{pmatrix} \tag{B.8}$$

$$h(q,\dot{q}) = \begin{pmatrix} -LM\sin\theta\,\dot{\theta}^2 + m(-L\sin\theta\,\dot{\theta}^2 + l\sin(\theta-\phi)(\dot{\theta}-\dot{\phi})^2 + l\cos(\theta-\phi)\ddot{\phi} \\ g(m+M) + LM\cos\theta\,\dot{\theta}^2 + m(L\cos\theta\,\dot{\theta}^2 - l\cos(\theta-\phi)(\dot{\theta}-\dot{\phi})^2 + l\sin(\theta-\phi)\ddot{\phi}) \\ g(L(m+M)\sin\theta - lm\sin(\theta-\phi) + lm(L\sin\phi(2\dot{\theta}-\dot{\phi})\dot{\phi} - (l-L\cos\phi)\ddot{\phi} \end{pmatrix} \tag{B.9}$$

B.1.0.2 Impact phase

From Sec: 4.1.2.2, conservation of angular momentum around the contact point during impact is used to calculate the state after impact.

$$\begin{aligned} \dot{\theta}^+ =& \frac{1}{J_L + l^2m + L^2(m+M) - 2lLm\cos\theta^-} \\ & \cdot \Big((L(m+M)\cos\theta - lm\cos(\theta^- - \phi^-))\dot{x}^- + (L(m+M)\sin\theta^- - lm\sin(\theta^- - \phi^-))\dot{y}^- \\ & + (J_L + l^2m + L^2(m+M) - 2lLm\cos\theta^-)\dot{\theta}^- - lm(l - L\cos\phi^-)(\dot{\phi}^- - \dot{\phi}^+) \Big) \end{aligned} \tag{B.10}$$

this last equation can further be simplified by noting that since there is a constraint trajectory $\dot{\phi}^- - \dot{\phi}^+ = 0$ and $\dot{\theta}^+$ reduces to

$$\begin{aligned} \dot{\theta}^+ = & \frac{1}{J_L + l^2m + L^2(m+M) - 2lLm\cos\theta^-} \\ & \cdot \Big((L(m+M)\cos\theta - lm\cos(\theta^- - \phi^-))\dot{x}^- + (L(m+M)\sin\theta^- - lm\sin(\theta^- - \phi^-))\dot{y}^- \\ & + (J_L + l^2m + L^2(m+M) - 2lLm\cos\theta^-)\dot{\theta}^- \Big) \end{aligned} \tag{B.11}$$

using this and the flip of coordinates during impact, the entire impact phase map is constructed

$$\begin{bmatrix} x^+ \\ y^+ \\ \theta^+ \\ \phi^+ \\ \dot{x}^+ \\ \dot{y}^+ \\ \dot{\theta}^+ \\ \dot{\phi}^+ \end{bmatrix} = \begin{bmatrix} -x^- \\ y^- \\ -\theta^- \\ -\phi^- \\ 0 \\ 0 \\ -\dot{\theta}^+ \\ -\dot{\phi}^- \end{bmatrix}, \tag{B.12}$$

where $\dot{\theta}^+$ is calculated using Eq. B.11.

B.1.0.3 Stance phase

Using the process described in Sec. 4.1.2.3, one can find the equations of motion of the mechanism and the contact forces from the wall. The problem can be decoupled when the leg is in contact with the wall, while keeping the no rebound, no slip assumption. Only the equations of motion for the $\theta, \dot{\theta}$ must be solved while observing the contact forces to see when they change sign, corresponding to transition to flight phase. The equations of motion for $\theta, \dot{\theta}$ are just the last (third) row of Eq. B.6

$$\begin{aligned}(J_L + l^2 m + L^2(m+M) - 2lLm\cos\phi)\ddot{\theta} + g(L(m+M)\sin\theta \\ - lm\sin(\theta-\phi) + lm(L\sin\phi(2\dot{\theta}-\dot{\phi})\dot{\phi} - (l - L\cos\phi)\ddot{\phi} = 0,\end{aligned} \tag{B.13}$$

The contact force is calculated using the Lagrange multipliers method. As in Eq. 4.10.

$$\lambda_{ext}(q,\dot{q}) = \left(A(q)M(q)^{-1}A(q)^T\right)^{-1}\left(\dot{A}(q)\dot{q} - A(q)M(q)^{-1}h(q,\dot{q})\right), \tag{B.14}$$

where $A(q) = \left(\begin{smallmatrix} 1 & 0 & 0 \\ 0 & 1 & 0 \end{smallmatrix}\right)$ and $M(q)$ and $h(q,\dot{q})$ are from Eq. B.7 and B.9.

B.2 Nondimensionalisation of the equations of motion

The conversion to nondimensional equations of motion is done by first picking the characteristic length to be d_{wall}, half of the wall gap. The non-dimensional variables are then picked to be

$$x^* = \frac{x}{d_{wall}}, \quad y^* = \frac{y}{d_{wall}}, \quad \theta^* = \theta, \quad \phi^* = \phi, \quad \tau = \omega t. \tag{B.15}$$

where $[.]^*$ represents the nondimensional variable and τ is the nondimensional time.

all the dimensional variables are replaced with their non-dimensional counterparts. Switching the configuration variables is trivial, e.g., $x = x^* d_{wall}$. In order to find the conversion for the velocities and acceleration the chain rule is used.

$$\begin{aligned}
\frac{dx}{dt} &= \frac{dx}{d\tau}\frac{d\tau}{dt} = d_{wall}\frac{dx^*}{d\tau}\frac{d\tau}{dt} = \omega\, d_{wall}\frac{dx^*}{d\tau} \\
\frac{dy}{dt} &= \frac{dy}{d\tau}\frac{d\tau}{dt} = d_{wall}\frac{dy^*}{d\tau}\frac{d\tau}{dt} = \omega\, d_{wall}\frac{dy^*}{d\tau} \\
\frac{d\theta}{dt} &= \frac{d\theta}{d\tau}\frac{d\tau}{dt} = \frac{d\theta^*}{d\tau}\frac{d\tau}{dt} = \omega\frac{d\theta^*}{d\tau} \\
\frac{d\phi}{dt} &= \frac{d\phi}{d\tau}\frac{d\tau}{dt} = \frac{d\phi^*}{d\tau}\frac{d\tau}{dt} = \omega\frac{d\phi^*}{d\tau}
\end{aligned} \tag{B.16}$$

Similarly the acceleration variables can be found

$$\begin{aligned}
\frac{d^2x}{dt^2} &= \omega^2\, d_{wall}\frac{d^2x^*}{d\tau^2} \\
\frac{d^2y}{dt^2} &= \omega^2\, d_{wall}\frac{d^2y^*}{d\tau^2} \\
\frac{d^2\theta}{dt^2} &= \omega^2\frac{d^2\theta^*}{d\tau^2} \\
\frac{d^2\phi}{dt^2} &= \omega^2\frac{d^2\phi^*}{d\tau^2}
\end{aligned} \tag{B.17}$$

After replacing the dimensional variables of Eq. B.6 with the nondimensional variables from Eqs. B.15, B.16, and B.17 the equations should be divided by one of the coefficients in order to normalize the equations. For simplicity we will normalize by $M(1,1)$. Since the third equation (corresponding to θ having units of $\frac{1}{T^2}$) is also divided by $M(1,1)$ (with units of $\frac{L}{T^2}$), we need to also divide this equation by the characteristic length. After these replacement and normalization we have the nondimensional matrix form of the general flight phase equations of motion

$$M^*(q^*)\ddot{q}^* + h^*(q^*, \dot{q}^*) = 0, \tag{B.18}$$

where

$$M^*(q^*) = \tag{B.19}$$

$$\begin{pmatrix} 1 & 0 & L^*\cos\theta^* - L^*l^*m^*\cos(\theta^*-\phi^*) \\ 0 & 1 & L^*\sin\theta^* - L^*l^*m^*\sin(\theta^*-\phi^*) \\ L^*\cos\theta^* - L^*l^*m^*\cos(\theta^*-\phi^*) & L^*\sin\theta^* - L^*l^*m^*\sin(\theta^*-\phi^*) & L^{*2}(1+J_L^*+l^{*2}m^*-2l^*m^*\cos\phi^*) \end{pmatrix} \tag{B.20}$$

$$h^*(q^*,\dot{q^*}) = \tag{B.21}$$

$$\begin{pmatrix} L^*\big((-\sin\theta^*+l^*m^*\sin(\theta^*-\phi^*))\dot{\theta^*}^2 - 2l^*m^*\sin(\theta^*-\phi^*)\dot{\theta}^*\dot{\phi}^* + l^*m^*(\sin(\theta^*-\phi^*)\dot{\phi^*}^2 + \cos(\theta^*-\phi^*)\ddot{\phi}^*)\big) \\ \gamma + L^*\big((\cos\theta^*-l^*m^*\cos(\theta^*-\phi^*))\dot{\theta^*}^2 + 2l^*m^*\cos(\theta^*-\phi^*)\dot{\theta}^*\dot{\phi}^* + L^*l^*m^*(-\cos(\theta^*-\phi^*)\dot{\phi^*}^2 + \sin(\theta^*-\phi^*)\ddot{\phi}^*)\big) \\ L^*\big(\gamma(\sin\theta^*-l^*m^*\sin(\theta^*-\phi^*)) + L^*l^*m^*(\sin\phi^*(2\dot{\theta}^*-\dot{\phi}^*)\dot{\phi}^* - l^* - \cos\phi^*)\ddot{\phi}^*)\big), \end{pmatrix} \tag{B.22}$$

where the nondimensional parameters are

$$m^* = \frac{m}{m+M}, \quad l^* = \frac{l}{L}, \quad L^* = \frac{L}{d_{wall}}, \quad J_L^* = \frac{J_L}{L^2(m+M)}, \quad \gamma = \frac{g}{d_{wall}\omega^2}, \tag{B.23}$$

Notice that these nondimensional parameters are not unique, we could have chosen other parameters such as $\frac{m}{M}$.

Continuing on the same note, we can produce nondimensional equations for the impact phase

$$\begin{aligned} \dot{\theta^*}^+ = {} & \frac{1}{L^*(1+J_L^*+l^{*2}m^*-2l^*m^*\cos\phi^*)} \\ & \cdot\Big((\cos\theta^{*-}-l^*m^*\cos(\theta^{*-}-\phi^{*-}))\dot{x}^{*-} + (\sin\theta^{*-}-l^*m^*\sin(\theta^{*-}-\phi^{*-}))\dot{y}^{*-} \\ & \qquad + L^*(1+J_L^*+L^*-2l^*m^*\cos\phi^*)\dot{\theta}^{*-}\Big) \end{aligned} \tag{B.24}$$

and the equation of motion for the stance phase

$$\begin{aligned} \big(L^{*2}(1+J_L^*+l^{*2}m^*-2l^*m^*\cos\phi^*)\big)\ddot{\theta}^* + L^*\big(\gamma(\sin\theta^*-l^*m^*\sin(\theta^*-\phi^*)) + \\ L^*l^*m^*(\sin\phi^*(2\dot{\theta}^*-\dot{\phi}^*)\dot{\phi}^* - l^* - \cos\phi^*\ddot{\phi}^*)\big) = 0, \end{aligned} \tag{B.25}$$

Bibliography

E. W. Aboaf, S. M. Drucker, and C. G. Atkeson. Task-level robot learning: Juggling a tennis ball more accurately. In *IEEE International Conference on Robotics and Automation*, pages 1290–1295, Scottsdale, AZ, 1989.

K. Autumn, M. Buehler, M. Cutkosky, R. Fearing, R. J. Full, D. Goldman, R. Groff, W. Provancher, A. A. Rizzi, U. Saranli, A. Saunders, and D. E. Koditschek. Robotics in scansorial environments. In *Proc. of SPIE Vol. 5804 Unmanned Ground Vehicle Technology VII*, pages 291–302, 2005.

M. D. Berkemeier and R. S. Fearing. Sliding and hopping gaits for the underactuated acrobot. *IEEE Transactions on Robotics and Automation*, 14(4):629–634, August 1998.

D. Bevly, S. Dubowsky, and C. Mavroidis. A simplified cartesian-computed torque controller for highly geared systems and its application to an experimental climbing robot. *Journal of Dynamic Systems, Measurement, and Control*, 122:27, 2000.

W. E. Boyce and R. C. DiPrima. *Elementary Differential Equations and Boundary Value Problems*. John Wiley & Sons, 2001.

T. Bretl. Motion planning of multi-limbed robots subject to equilibrium constraints: The free-climbing robot problem. *The International Journal of Robotics Research*, 25(4):317–342, 2006.

H. B. Brown, Jr. and G. Zeglin. The bow leg hopping robot. In *IEEE International Conference on Robotics and Automation*, pages 781–786, 1998.

M. Bühler and D. E. Koditschek. From stable to chaotic juggling: Theory, simulation, and experiments. In *IEEE International Conference on Robotics and Automation*, pages 1976–1981, Cincinnati, OH, 1990.

J.F. Canny and K.V. Goldberg. A RISC approach to sensing and manipulation. *Journal of Robotic Systems*, 12(6), 1995.

J. E. Clark, D. I. Goldman, T. S. Chen, R. J. Full, and D. Koditschek. Toward a dynamic climbing robot. In *Proc. of the 9th International Conference on Climbing and Walking Robots (CLAWAR '06)*, Brussels, Belguim, September 2006.

J.E. Clark, D.I. Goldman, P.C. Lin, and G. Lynch. Design of a Bio-inspired Dynamical Vertical Climbing Robot. *Robotics: Science and Systems III Atlanta, Georgia*, 2007.

S. Collins, A. Ruina, R. Tedrake, and M. Wisse. Efficient bipedal robots based on passive-dynamic walkers. *Science*, 307(5712):1082–1085, February 2005.

S. H. Collins, M. Wisse, and A. Ruina. A three-dimensional passive-dynamic walking robot with two legs and knees. *International Journal of Robotics Research*, 20(7):607–615, July 2001.

M. A. Erdmann and M. T. Mason. An exploration of sensorless manipulation. *IEEE Transactions on Robotics and Automation*, 4(4):369–379, August 1988.

M. Garcia, A. Chatterjee, A. Ruina, and M. Coleman. The simplest walking model: stability, complexity, and scaling. *Journal of Biomechanical Engineering*, 120(2):281–288, April 1998.

M.W. Gomes and A. Ruina. A walking model with no energy cost. *Journal of Theoretical Biology*, 2005.

A. Goswami, B. Thuilot, and B. Espiau. A study of the passive gait of a compass-like biped robot: symmetry and chaos. *The International Journal of Robotics Research*, 17(12):1282, 1998.

A. Greenfield, A. A. Rizzi, and H. Choset. Dynamic ambiguities in frictional rigid-body systems with application to climbing via bracing. In *Proc. of the IEEE International Conference on*

Robotics and Automation, (ICRA '05), pages 1947– 1952, Barcelona, Spain, 2005.

D. T. Greenwood. *Classical dynamics*. Dover Publications, Mineola, N.Y., 1997.

J. Guckenheimer and P. Holmes. *Nonlinear Oscillations, Dynamical Systems, and Bifurcations of Vector Fields*. Springer, 1983.

J. K. Hodgins and M. H. Raibert. Biped gymnastics. *International Journal of Robotics Research*, 9(2):115–132, 1990.

C.S Hsu. *Cell-to-cell mapping: a method of global analysis for nonlinear systems*. Springer, New York, 1997.

S. Kim, A. T. Asbeck, M. R. Cutkosky, and W. R. Provancher. SpinybotII: Climbing hard walls with compliant microspines. In *Proc. of the 12th International Conference on Advanced Robotics, (ICAR '05)*, pages 601–606, Seattle, WA, 2005.

S. Kim, M. Spenko, S. Trujillo, B. Heyneman, V. Mattoli, and M. R. Cutkosky. Whole body adhesion: hierarchical, directional and distributed control of adhesive forces for a climbing robot. In *IEEE International Conference on Robotics and Automation*, pages 1268–1273, 2007.

D. E. Koditschek and M. Bühler. Analysis of a simplified hopping robot. *International Journal of Robotics Research*, 10(6):587–605, December 1991.

D. Longo and G. Muscato. The Alicia^3 climbing robot. *IEEE Robotics and Automation Magazine*, 13:2–10, 2006.

K. M. Lynch and Craig K. Black. Recurrence, controllability, and stabilization of juggling. *IEEE Transactions on Robotics and Automation*, 17(2):113–124, April 2001.

K.M. Lynch and M.T. Mason. Dynamic nonprehensile manipulation: Controllability, planning, and experiments. *International Journal of Robotics Research*, 1999.

T. McGeer. Passive walking with knees. In *IEEE International Conference on Robotics and Automation*, pages 1640–1645, 1990a.

T. McGeer. Passive dynamic walking. *The International Journal of Robotics Research*, 9(2): 62–82, April 1990b.

K. D. Mombaur, H. G. Bock, J. P. Schloder, and R. W. Longman. Self-stabilizing somersaults. *IEEE Transactions on Robotics*, 21(6):1148–1157, December 2005a.

K.D. Mombaur, R.W. Longman, H.G. Bock, and J.P. Schlöder. Open-loop stable running. *Robotica*, 23(01):21–33, 2005b.

R. M. Murray, Z. Li, and S. S. Sastry. *A Mathematical Introduction to Robotic Manipulation*. CRC Press, Boca Raton, FA, 1994.

NaturalPoint™. Optitrack camera system. Retrieved from http://www.naturalpoint.com/optitrack, July 2009.

A.H. Nayfeh and B. Balachandran. *Applied nonlinear dynamics*. Wiley New York, 1995.

T.S. Parker and L.O. Chua. *Practical numerical algorithms for chaotic systems*. Springer-Verlag New York, Inc. New York, NY, USA, 1989.

M. H. Raibert. *Legged Robots That Balance*. The MIT Press, Cambridge, MA, 1986.

M. H. Raibert and H. B. Brown, Jr. Experiments in balance with a 2D one-legged hopping machine. *ASME Journal of Dynamic Systems, Measurement, and Control*, 106:75–81, 1984.

M. H. Raibert, H. B. Brown, Jr., and M. Chepponis. Experiments in balance with a 3D one-legged hopping machine. *International Journal of Robotics Research*, 3:75–92, 1984.

M. H. Raibert, M. Chepponis, and H. B. Brown, Jr. Running on four legs as though they were one. *IEEE Journal on Robotics and Automation*, 2:70–82, 1986.

R. Ringrose. Self-stabilizing running. In *IEEE International Conference on Robotics and Automation*, pages 487–493, 1997.

A. A. Rizzi and D. E. Koditschek. Progress in spatial robot juggling. In *IEEE International Conference on Robotics and Automation*, pages 775–780, Nice, France, 1992.

R. Ronsse, P. Lefevre, and R. Sepulchre. Sensorless stabilization of bounce juggling. *IEEE Transactions on Robotics*, 22(1):147–159, February 2006.

U. Saranli, M. Bühler, and D. E. Koditschek. RHex: A simple and highly mobile hexapod robot. *International Journal of Robotics Research*, 20(7):616–631, 2001.

A. Shapiro, E. Rimon, and S. Shoval. PCG: A foothold selection algorithm for spider robot locomotion in 2D tunnels. *The International Journal of Robotics Research*, 24(10):823–844, 2005.

J.C. Sprott. *Chaos and Time-Series Analysis*. Oxford University Press, 2003.

DE Stewart and JC Trinkle. An implicit time-stepping scheme for rigid body dynamics with inelastic collisions and coulomb friction. *International Journal for Numerical Methods in Engineering*, 39(15), 1996.

A. F. Vakakis, J. W. Burdick, and T. K. Caughey. An interesting strange attractor in the dynamics of a hopping robot. *International Journal of Robotics Research*, 10(6):606–618, December 1991.

G. Zeglin and H. B. Brown, Jr. Control of a bow leg hopping robot. In *IEEE International Conference on Robotics and Automation*, pages 793–798, 1998.